SUPPLEMENTARY INFORMATION FOR

Block copolymer micelles as colloidal catalysts for photocatalytic NAD^+ reduction

Jonas Eichhorn[1,2], Alexander K. Mengele[3], Christof Neumann[2,4,5], Johannes Biskupek[6], Sven Rau[3], Andrey Turchanin[2,4,5], Ute Kaiser[6], and Felix H. Schacher[1,2,5]*

[1] Institute of Organic Chemistry and Macromolecular Chemistry (IOMC), Friedrich Schiller University Jena, Humboldtstraße 10, 07743 Jena, Germany
felix.schacher@uni-jena.de;

[2] Jena Center for Soft Matter (JCSM), Friedrich Schiller University Jena, Philosophenweg 7, 07743 Jena, Germany

[3] Institute of Inorganic Chemistry I, Ulm University, Albert-Einstein-Allee 11, 89081 Ulm, Germany

[4] Institute of Physical Chemistry and Abbe Center of Photonics, Friedrich Schiller University Jena, Lessingstraße 10, 07743 Jena, Germany

[5] Center for Energy and Environmental Chemistry Jena (CEEC Jena), Philosophenweg 7a, 07743 Jena, Germany

[6] Electron Microscopy of Materials Science, Central Facility for Electron Microscopy, Ulm University, Albert-Einstein-Allee 11, 89081 Ulm, Germany

* Corresponding author

CONTENTS

S1 General Information

Materials

Potassium hexafluorophosphate (≥99 %), L-ascorbic acid (99 %), pentamethylcyclopentadienyl rhodium(III) chloride dimer $[Rh(Cp^*)Cl_2]_2$ (97 %) and *cis*-bis(2,2'-bipyridine)dichlororuthenium(II) hydrate (97 %) were purchased from Sigma-Aldrich (Steinheim, Germany). *tert*-Butyl acrylate (99 %) was purchased from Alfa Aesar (Kandel, Germany), trifluoroacetic acid (99.9 %) was purchased from abcr GmbH (Karlsruhe, Germany) and 4,4'-dimethyl-2,2-bipyridine (99.82 %) was purchased from BLD Pharmatech Ltd. (Shanghai, China). Ammonium molybdate(VI) tetrahydrate (>99 %) was purchased from Acros Organics (Geel, Belgium). All chemicals were used as received. Bis(2,2'-bipyridine)-bis(acetonitrile)ruthenium-(II) hexafluoro-phosphate ($[Ru(bpy)_2(ACN)_2](PF_6)_2$) was synthesized as described elsewhere. Polymerization inhibitor was removed from *tert*-butyl acrylate by passing over a short column of basic aluminum oxide. All deuterated solvents were purchased from Eurisotop or Deutero.

Characterization

Nuclear magnetic resonance (NMR). Measurements were performed on a 300 MHz *Bruker Avance I* or 500 MHz *Bruker Avance IV*. The chemical shift for ^{1}H-NMR experiments is referenced to tetramethylsilane (TMS). The solvent used is always specified and the spectra were referenced to the solvent signal. The obtained NMR spectra were analyzed with the program *MestReNova*.

Size exclusion chromatography (SEC). For [Ru]-containing polymers SEC analysis was carried out on a *Shimadzu System*, that was equipped with a *SCL-10A vp* controller, a *DGU-14A* degasser, a *LC-10AD vp* pump, a *SIL-10AD vp* autosampler, a *CTO-10AC vp* oven, a *RID-10A* refractive index detector and an *SPD-10MA vp* diode array detector. DMAC + 0.08 wt.% NH_4PF_6 was used as the eluent at a flow rate of 1 mL/min on a *Phenomenex Phenogel guard/100,000/1,000 Å* (10 µm particle size with a separation range from 400 – 1,000,000 g/mol) as stationary phase. The system was calibrated on a polystyrene standard from *PSS (Mainz, Deutschland)* and the measurement was performed at 40 °C. The analysis of the obtained data from RI detection was carried out with the program *PSS WinGPC® UniChrom*. Diode array data was baseline corrected. Therefore, for each wavelength a cubic spline fit function was applied assuming at 5.0, 12.0 and 26.3 mL elution volumes no sample absorption. SEC analysis of polymers without incorporated [Ru] was carried out on an *Agilent System (1260 series)*, that was equipped with a *PSS* degasser, a *G1330B* pump, a *G1362A* refractive index detector and a *G1315D* diode array detector. THF was used as the eluent at a flow rate of 1 mL/min on a *PSS SDV guard/100/1,000/100,000 Å (5 µm particle size* with a separation range from 400 – 2,520,000 g/mol) as stationary phase. The system was calibrated on a polystyrene standard from *PSS (Mainz, Deutschland)*

and the measurement was performed at 30 °C. The analysis of the obtained data was carried out with the program *PSS WinGPC® UniChrom*.

X-ray photoelectron spectroscopy (XPS). The samples for XPS analysis were prepared *via* drop casting of the dissolved substances in *N*,*N*-dimethylformamide onto a precleaned Au/Si wafer. After drying at ambient conditions, the samples were introduced for the XPS measurements into a UHV multiprobe system (*Scienta Omicron*) with a monochromatic X-ray source (Al K_α) and an electron analyzer (*Argus CU*) with a 0.6 eV spectral energy resolution. For individual samples, charge compensation during data acquisition was realized by an electron flood gun (*NEK150, Staib*, Germany) at 6 eV and 50 µA. The spectra were fitted using Voigt functions after background subtraction. The spectra were afterwards calibrated using the aromatic C 1s peak at 284.6 eV and the Au $4f_{7/2}$ peak at 84.0 eV, respectively. The absolute intensities of signals may vary between the different samples, as the amount of dried substances within the measurement spot (~1-2 mm²) can be different. Therefore, the different samples are only compared qualitatively.

Dynamic light scattering (DLS). Measurements were performed with the *ALV/CGS-3 Compact Goniometer System*. The measurement was accomplished under the usage of a laser (λ = 633 nm) at a temperature of 25 °C at a detection angle of 90 °. As correlator the device *ALV/LSE-5004* was utilized. The analysis of the obtained data was carried out with *ALV-Correlator 3.0* software. Prior to the DLS measurement the sample was filtered over a glass filter (pore size: 1 µm).

Transmission electron microscopy (TEM).

For TEM copper grids were rendered hydrophilic by Ar plasma cleaning for 30 s (*Diener Electronics*). 10 µL of the respective sample solution were applied to the grid and excess sample was blotted with a filter paper. TEM images were acquired with a 200 kV *FEI Tecnai G2 20* equipped with a 4k x 4k *Eagle HS* CCD and a 1k x 1k *Olympus MegaView* camera for overview images. Data processing as well as the determination of the core radius of micelles (individually measuring area of 40 separated and spherical micelles each sample) was performed with the program *ImageJ*. For determining the aggregation number (N_{agg}) the measured core radius (r_{core}) was used as basis:

$$N_{agg} = \frac{m_{core}}{m_{PS}^{chain}} = \frac{4\pi N_A \rho_{PS} r_{core}^{\ 3}}{3M_{PS}^{chain}}$$

with m_{core}: mass of the micellar core; m_{PS}^{chain} : mass of an individual PS chain; N_A: Avogadro constant; ρ_{PS}: density of polystyrene; r_{core}: radius of the micellar core according to TEM; M_{PS}^{chain} : molecular weight of an individual PS chain. In a study by EISENBERG et al. about 6 % of the micellar radius in the dry-state were attributed to the hydrophilic segment of PS_{1400}-*b*-PAA_{310}.[1] Although such asymmetry in block ratio is not given for the [Rh] block copolymer, the calculation of average radii of the PS core ($\bar{r}_{core}$) on the basis of TEM images was conducted on the assumption that a determined radius in TEM

analysis is equal to $\bar{r}_{core}$. In conclusion, values for $\bar{r}_{core}$, average aggregation number ($\bar{N}_{agg}$) and mean chain density on the core surface ($\bar{\rho}_{chain}$) differ from reality but allow a qualitative comparison of the obtained results.

Scanning transmission electron microscopy and energy-dispersive X-ray spectroscopy (STEM-EDX).

STEM imaging with parallel acquisition of EDX spectra was acquired *via* a *Thermofisher Talos 200X* (S)TEM operating at 200 kV. The microscopy was equipped with *4-quadrant SuperX*. To avoid carbon contamination in the scanned sample areas, the micellar solutions were drop-casted on 20 nm thin SiN film grids (Plano GmbH) followed by reactive oxygen plasma (*Fishione Nanoclean 1070*) to the remove respectively to immobilize hydrocarbons.

UV/vis spectroscopy. Measurements were performed on an *Agilent Cary 60* in a *Hellma* quartz glass cuvette with a pathlength of 10 mm at room temperature in the respective solvent. The absorbance was measured in a range from 200 nm to 800 nm in 1 nm steps.

S2 Synthesis

The synthesis of *N*-*tert*-butyl-*N*-(1-(diethoxyphosphoryl)-2,2-dimethylpropyl-*N*-oxyl nitroxide (SG1), polystyrene (PS) macroinitiator and 2-(4-(4'-methyl-2,2'-bipyridyl))ethylacrylate (bpyEA) was carried out analogously to literature.[2]

PS-*b*-P(*t*BuA-*co*-bpyEA) block copolymers

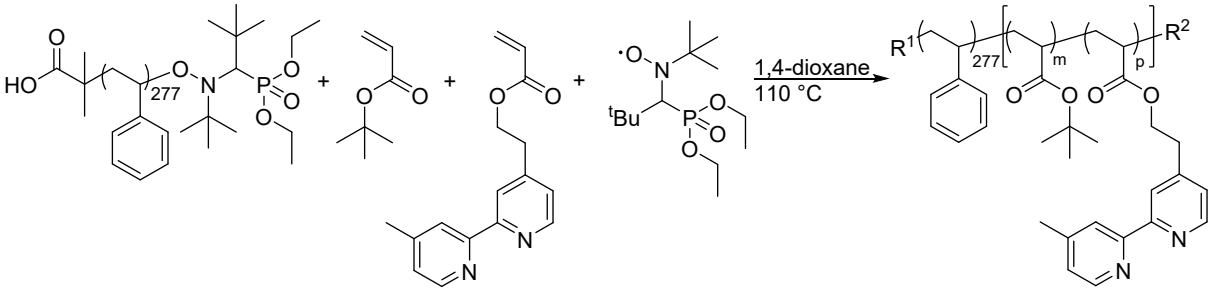

Scheme S1: Block extension of PS_{277} with *t*BuA and 10 mol% bpyEA, M/I = 800:1, R^1 = 1,1-dimethyl-2-carboxyethyl, R^2 = SG1; m = 99, p = 9 for 7 hours of reaction time; m = 262, p = 28 for 16 hours of reaction time.

The PS-*b*-P(*t*BuA-*co*-bpyEA) block copolymers were prepared in an adapted procedure previously published.[2] Therefore, 200 mg (3.425 µmol) polystyrene macroinitiator (PS_{277}, $M_n = 29{,}200\,\frac{g}{mol}\,(SEC)$, $Đ = 1.07\,(SEC)$), 632 mg (4.93 mmol) *t*BuA and 147 mg (0.55 mmol) bpyEA as well as 0.12 mg (0.12 µL, 0.41 µmol) SG1 were dissolved in 2 mL 1,4-dioxane and heated at 110 °C for 7 and 16 h, respectively. Subsequently, the reaction mixture was diluted with 4 mL of THF and the block copolymer was precipitated three times in a mixture of methanol/water (9:1). Afterwards, the block copolymer was dissolved in 1,4-dioxane and freeze dried to yield the block copolymer as a pale-yellow powder. PS_{277}-*b*-P(*t*BuA_{99}-*co*-$bpyEA_9$) (**BCP1**): Yield: 293 mg. ^{1}H-NMR: (300.13 MHz, CD_2Cl_2, 300.0 K): δ [ppm] 8.61-8.20 (aromatic for bpyEA), 7.32-6.33 (aromatic for styrene and bpyEA), 4.31 (C_{ar}-CH_2-CH_2O- for bpyEA), 3.05 (C_{ar}-CH_2-CH_2O- for bpyEA), 2.44 (C_{ar}-CH_3 for bpyEA), 2.31-1.06 (backbone, -O-C(CH_3)$_3$ for *t*BuA). $\bar{M}_n = 44{,}300\,\frac{g}{mol}\,(NMR).\,Đ = 1.16\,(SEC)$. PS_{277}-*b*-P(*t*BuA_{262}-*co*-$bpyEA_{28}$) (**BCP2**): Yield: 464 mg. ^{1}H-NMR: (300.13 MHz, CD_2Cl_2, 300.0 K): δ [ppm] 8.60-8.15 (aromatic for bpyEA), 7.30-6.30 (aromatic for styrene and bpyEA), 4.30 (C_{ar}-CH_2-CH_2O- for bpyEA), 3.04 (C_{ar}-CH_2-CH_2O- for bpyEA), 2.42 (C_{ar}-CH_3 for bpyEA), 2.33-1.00 (backbone, -O-C(CH_3)$_3$ for *t*BuA). $M_n = 70{,}400\,\frac{g}{mol}\,(NMR).\,Đ = 1.28\,(SEC)$.

Chloro(4,4'-dimethyl-2,2'-bipyridine)pentamethylcyclopentadienylrhodium(III)chloride [Rh(dmbpy)(Cp*)Cl]Cl (1)

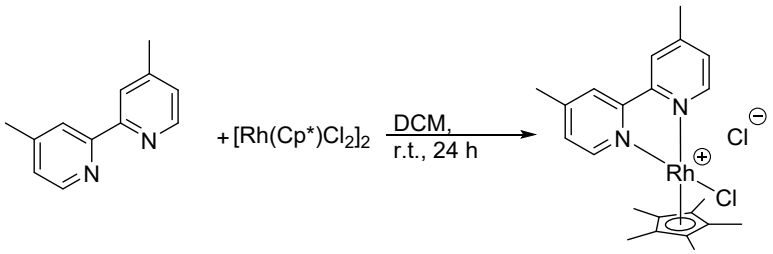

Scheme S2: Synthesis of [Rh(dmbpy)(Cp*)Cl]Cl.

A mixture of 100 mg (162 µmol) $[Rh(Cp^*)Cl_2]_2$ and 71.6 mg (388 µmol) 4,4'-dimethyl-2,2'-bipyridine in 10 mL DCM was stirred for 24 h at room temperature. Subsequently, the solvent was removed under reduced pressure. The orange-brown residue was dissolved in a small portion of methanol and *via* slow diffusion of diethyl ether orange crystals as product were obtained. Yield: 170 mg (89 %). ^{1}H-NMR: (300.13 MHz, CD_2Cl_2, 300.0 K): δ [ppm] 8.67 (d, ^3J(H-H) = 5.7 Hz, 2H, *H*-6, dmbpy), 8.53-8.52 (m, 2H, *H*-3), 7.60 (dd, ^3J(H-H) = 5.7 Hz, ^4J(H-H) = 1.3 Hz, 2H, *H*-5), 2.64 (s, 6H, -CH_3 dmbpy), 1.70 (s, 15H, -CH_3 Cp*).

PS-*b*-P(*t*BuA-*co*-([Rh(bpyEA)(Cp*)Cl]Cl)) block copolymers

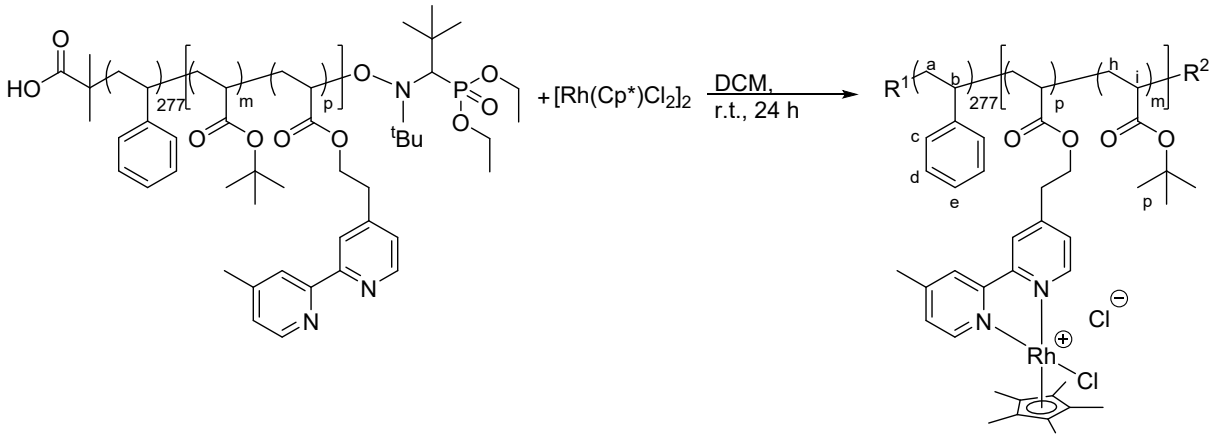

Scheme S3: Functionalization of PS-*b*-P(*t*BuA-*co*-bpyEA) block copolymers with $[Rh(Cp^*)Cl_2]_2$, R^1 = 1,1-dimethyl-2-carboxyethyl, R^2 = SG1.

A solution of 50.0 mg PS-*b*-P(*t*BuA-*co*-bpyEA) block copolymer and the respective amount (**Table S1**) of $[Rh(Cp^*)Cl_2]_2$ in 1 mL DCM was stirred overnight at room temperature. Afterwards, the orange-colored reaction mixture was purified by gel permeation chromatography (Biobeads SX-1, DCM). The high molecular orange colored fraction was collected and freed from all volatiles before being dissolved in 1,4-dioxane for freeze-drying. A pale orange powder was obtained as product.

Table S1: Batch calculation and selected analytical data for PS-*b*-P(*t*BuA-*co*-([Rh(bpyEA)(Cp*)Cl]Cl)) block copolymers.

Starting material	$[Rh(Cp^*)Cl_2]_2$ [mg (mmol)]	$\bar{M}_n$ [g/mol][a]	Yield [mg]
PS_{277}-*b*-P(^{t}BuA_{99}-*co*-bpyEA$_9$) (**BCP1**)	10.5 (17.0)	47,100	57
PS_{277}-*b*-P(^{t}BuA_{262}-*co*-bpyEA$_{28}$) (**BCP2**)	14.9 (24.2)	79,000	48

[a] NMR analysis.

PS_{277}-*b*-P(^{t}BuA_{99}-*co*-([Rh(bpyEA)(Cp*)Cl]Cl)$_9$) (**[Rh]@BCP1**): ^{1}H-NMR: (300.13 MHz, CD_2Cl_2, 300.0 K): δ [ppm] 8.92-8.28 (m, 4H, *H*-3, *H*-6, [Rh(bpyEA)(Cp*)Cl]Cl), 7.84-7.48 (m, 2H, *H*-5, [Cp*Rh(bpyEA)Cl]Cl), 7.40-6.30 (m, aromatic for styrene), 4.50-4.29 (m, C_{ar}-C*H*$_2$-CH$_2$O- for [Rh(bpyEA)(Cp*)Cl]Cl), 3.33-3.11 (m, C_{ar}-CH$_2$-C*H*$_2$O- for [Rh(bpyEA)(Cp*)Cl]Cl), 2.63 (s, C_{ar}-C*H*$_3$ for [Rh(bpyEA)(Cp*)Cl]Cl), 2.41-1.00 (backbone, -O-C(C*H*$_3$)$_3$ for ^{t}BuA, -C*H*$_3$ for Cp*). PS_{277}-*b*-P(^{t}BuA_{262}-*co*-([Rh(bpyEA)(Cp*)Cl]Cl)$_{28}$) (**[Rh]@BCP2**): ^{1}H-NMR: (300.13 MHz, CD_2Cl_2, 300.0 K): δ [ppm] 9.10-8.41 (m, 4H, *H*-3, *H*-6, [Rh(bpyEA)(Cp*)Cl]Cl), 7.82-7.51 (m, 2H, *H*-5, [Rh(bpyEA)(Cp*)Cl]Cl), 7.30-6.31 (m, aromatic for styrene), 4.56-4.23 (m, C_{ar}-C*H*$_2$-CH$_2$O- for [Rh(bpyEA)(Cp*)Cl]Cl), 3.44-3.05 (m, C_{ar}-CH$_2$-C*H*$_2$O- for [Rh(bpyEA)(Cp*)Cl]Cl), 2.36 (C_{ar}-C*H*$_3$ for [Rh(bpyEA)(Cp*)Cl]Cl), 2.41-1.01 (backbone, -O-C(C*H*$_3$)$_3$ for ^{t}BuA, -C*H*$_3$ for Cp*).

PS-*b*-P(AA-*co*-([Rh(bpyEA)(Cp*)Cl]CF_3CO_2)) block copolymers

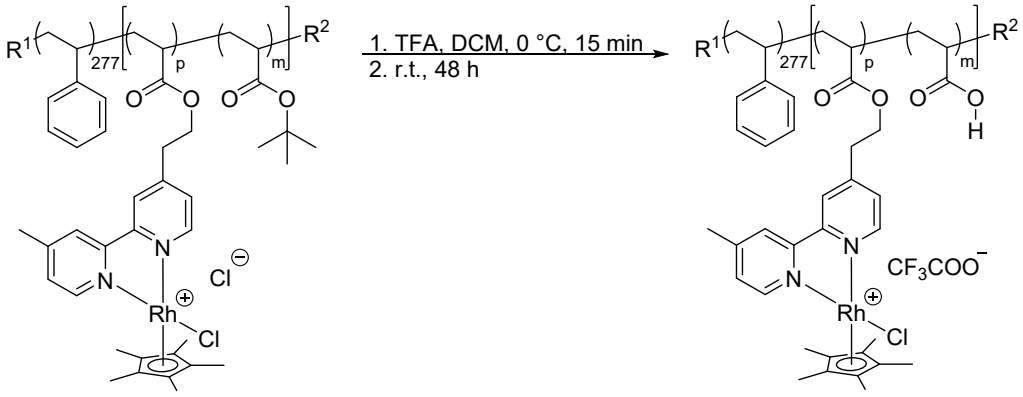

Scheme S4: Functionalization of PS-*b*-P(^{t}BuA-*co*-bpyEA) block copolymers with $[Cp^*RhCl_2]_2$, R^1 = 1,1-dimethyl-2-carboxyethyl, R^2 = SG1.

The respective amount of the PS-*b*-P(^{t}BuA-*co*-([Rh(bpyEA)(Cp*)Cl]Cl)) block copolymer was dissolved in 0.5 mL dry DCM and the respective amount of TFA was added at 0°C. After stirring for 15 min the ice bath was removed and stirring was continued for 48 h at room temperature. Afterwards, the orange-colored reaction mixture was purified by gel permeation chromatography (Biobeads SX-1, DCM). The high molecular orange colored fraction was collected and freed from all volatiles before being dissolved in 1,4-dioxane for freeze-drying. A pale orange powder was obtained as product.

Table S2: Batch calculation and selected analytical data for PS-*b*-P(*t*BuA-*co*-([Rh(bpyEA)(Cp*)Cl]Cl)) block copolymers.

Starting material	Starting material [mg (mmol)]	TFA [mg (mmol)]	M_n [g/mol][a]	Yield [mg]
PS_{277}-*b*-P(^{t}BuA_{99}-*co*-([Rh(bpyEA)(Cp*)Cl]Cl)$_9$) (**[Rh]@BCP1**)	35.0 (0.74)	169 (1.48)	41,600	21
PS_{277}-*b*-P(^{t}BuA_{262}-*co*-([Rh(bpyEA)(Cp*)Cl]Cl)$_{28}$) (**[Rh]@BCP2**)	25.0 (0.32)	195 (1.71)	64,300	15

[a] NMR analysis.

PS_{277}-*b*-P(AA_{99}-*co*-([Rh(bpyEA)(Cp*)Cl]Cl)$_9$) (**[Rh]@BCP3**): ^{1}H-NMR: (300.13 MHz, CD_2Cl_2, 300.0 K): δ [ppm] 8.92-8.28 (m, 4H, *H*-3, *H*-6, [Rh(bpyEA)(Cp*)Cl]Cl), 7.84-7.48 (m, 2H, *H*-5, [Rh(bpyEA)(Cp*)Cl]Cl), 7.40-6.30 (m, aromatic for styrene), 4.50-4.29 (m, C_{ar}-CH_2-CH_2O- for [Rh(bpyEA)(Cp*)Cl]Cl), 3.33-3.11 (m, C_{ar}-CH_2-CH_2O- for [Rh(bpyEA)(Cp*)Cl]Cl), 2.63 (s, C_{ar}-CH_3 for [Rh(bpyEA)(Cp*)Cl]Cl), 2.41-1.00 (backbone, -O-C(CH_3)$_3$ for ^{t}BuA, -CH_3 for Cp*). PS_{277}-*b*-P(AA_{262}-*co*-([Rh(bpyEA)(Cp*)Cl]Cl)$_{28}$) (**[Rh]@BCP4**): ^{1}H-NMR: (300.13 MHz, CD_2Cl_2, 300.0 K): δ [ppm] 9.10-8.41 (m, 4H, *H*-3, *H*-6, [Rh(bpyEA)(Cp*)Cl]Cl), 7.82-7.51 (m, 2H, *H*-5, [Rh(bpyEA)(Cp*)Cl]Cl), 7.30-6.31 (m, aromatic for styrene), 4.56-4.23 (m, C_{ar}-CH_2-CH_2O- for [Rh(bpyEA)(Cp*)Cl]Cl), 3.44-3.05 (m, C_{ar}-CH_2-CH_2O- for [Rh(bpyEA)(Cp*)Cl]Cl), 2.36 (C_{ar}-CH_3 for [Rh(bpyEA)(Cp*)Cl]Cl), 2.41-1.01 (backbone, -O-C(CH_3)$_3$ for ^{t}BuA, -CH_3 for Cp*).

Bis(2,2'-bipyridine)-(4,4'-dimethyl-2,2'-bipyridine)ruthenium-(II) hexafluorophosphate ($[Ru(bpy)_2(dmbpy)](PF_6)_2$) (2)

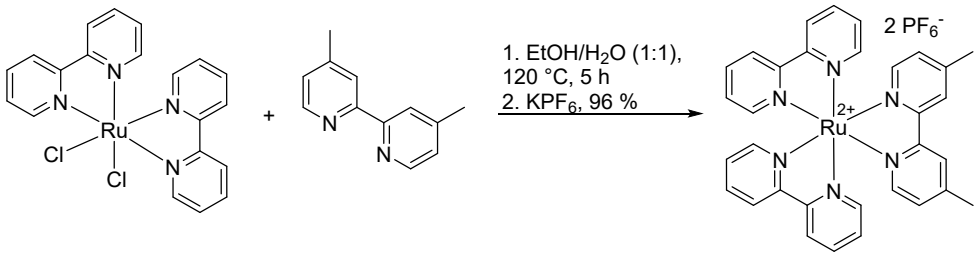

Scheme S5: Synthesis of $[Ru(bpy)_2(dmbpy)](PF_6)_2$.

Bis(2,2'-bipyridine)-(4,4'-dimethyl-2,2'-bipyridine)ruthenium-(II) hexafluorophosphate ($[Ru(bpy)_2(dmbpy)](PF_6)_2$) was synthesized according to a literature report.[3] A mixture of 100.0 mg (206 µmol) *cis*-bis(2,2′-bipyridine)-dichlororuthenium(II) hydrate and 38.0 mg (206 µmol) 4,4'-dimethyl-2,2'-bipyridine in 4 mL ethanol/water (1:1) was degassed with argon for 30 min before being heated at 120°C for 5 hours in a 20 mL microwave vial. After cooling to room temperature black residues were removed by centrifugation and the orange-red colored reaction solution was dropped into

3 mL of aqueous, saturated KPF_6 solution. The orange precipitate was removed *via* centrifugation and washed with water (10 mL), cold ethanol (5 mL) and diethyl ether (Et_2O, 10 mL). Recrystallization from DCM and Et_2O (diffusion crystallization) afforded 176 mg of $([Ru(bpy)_2(dmbpy)](PF_6)_2$ containing 51 mg residual Et_2O as red-orange crystals. Yield: 125 mg (77%). ^{1}H-NMR: (300.13 MHz, DMF-d_7, 300.0 K): δ [ppm] 8.95 (d, ^3J(H-H) = 8.1 Hz, 4H, *H*-3 bpy), 8.85-8.82 (m, 2H, *H*-3 dmbpy), 8.24 (ddt, ^3J(H-H) = 7.9, 3.4 Hz, ^4J(H-H) = 1.5 Hz, 4H, *H*-4 bpy), 8.06-8.00 (m, 4H, *H*-6 bpy, DMF-d_7 solvent signal), 7.83 (d, ^3J(H-H) = 5.7 Hz, 2H, *H*-6 dmbpy), 7.62 (dtd, ^3J(H-H) = 7.6, 5.5 Hz, ^4J(H-H) = 1.3 Hz, 4H, *H*-5 bpy), 7.47 (ddd, ^3J(H-H) = 5.8 Hz, ^4J(H-H) = 1.9, 0.8 Hz, 2H, *H*-5 dmbpy), 3.51 (s, water), 3.41 (q, ^3J(H-H) = 7.0 Hz, diethyl ether) 2.42 (C_{ar}-C*H*$_3$ dmbpy), 1.11 (t, ^3J(H-H) = 7.0 Hz, diethyl ether).

Attachment of [Ru] to PS-*b*-P(^{t}BuA-*co*-bpyEA)

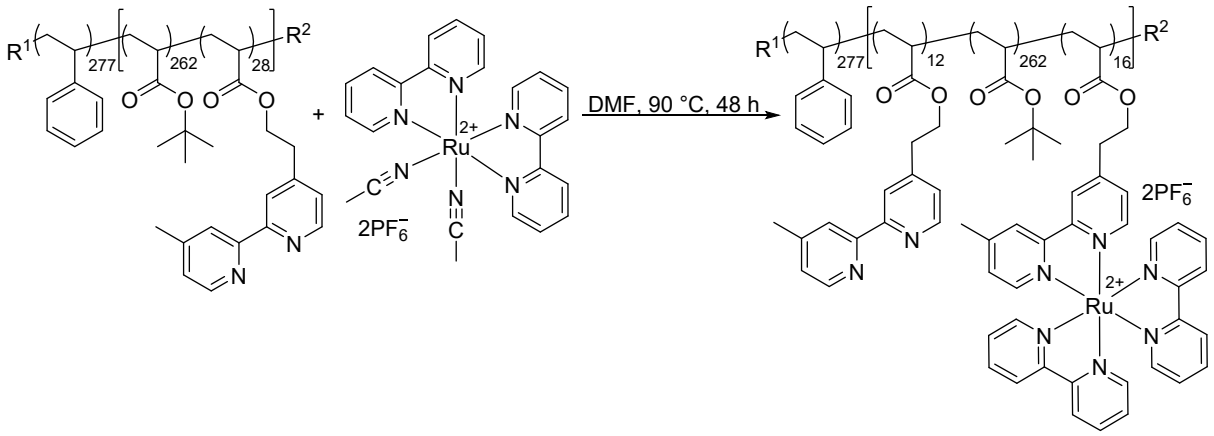

Scheme S6: Synthesis of PS_{277}-*b*-P(^{t}BuA_{262}-*co*-bpyEA_{12}-*co*-([Ru(bpyEA)(bpy)$_2$](PF$_6$)$_2$)$_{16}$) (**[Ru]@BCP2**), R^1 = 1,1-dimethyl-2-carboxyethyl, R^2 = SG1.

A mixture of 50.0 mg (1.42 µmol) **BCP2** and 19.0 mg (24.15 µmol) $[Ru(bpy)_2(ACN)_2](PF_6)_2$ in 1 mL DMF was degassed with argon for 20 min before being stirred at 90 °C for 48 h. Afterwards, the reaction solution was diluted with 5 mL DCM and purified by size exclusion chromatography (Biobeads SX-1, DCM). The orange colored, high molecular weight fraction was collected. Subsequently, all volatiles were removed under reduced pressure and the residue was dissolved in 1,4-dioxane prior to freeze-drying yielding an orange power as product. Yield: 56 mg. ^{1}H-NMR: (300.13 MHz, CD_2Cl_2, 300.0 K): δ [ppm] 8.65-8.34 (aromatic for bpyEA, [Ru]), 8.33-8.19 (aromatic for bpyEA), 7.78-7.39 (aromatic for [Ru]), 7.33-6.30 (aromatic for styrene, [Ru] and bpyEA), 4.48-4.07 (C_{ar}-C*H*$_2$-CH$_2$O- for bpyEA and [Ru]), 3.25-2.97 (C_{ar}-CH$_2$-C*H*$_2$O- for bpyEA and [Ru]), 2.58 (C_{ar}-C*H*$_3$ for [Ru]), 2.44 (C_{ar}-C*H*$_3$ for bpyEA) 2.36-1.00 (backbone, 1.43 (-O-C(C*H*$_3$)$_3$ for ^{t}BuA). Degree of functionalization with [Ru]: 57 mol%.

PS-*b*-P(AA-*co*-bpyEA-*co*-([Ru(bpy)$_2$(bpyEA)](CF$_3$CO$_2$)$_2$))

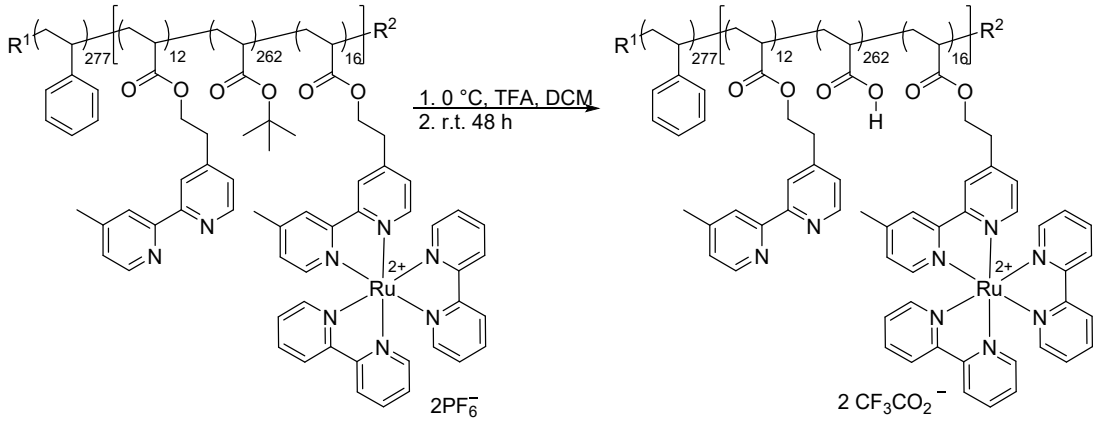

Scheme S7: Synthesis of PS$_{277}$-*b*-P(AA$_{262}$-*co*-bpyEA$_{12}$-*co*-([Ru(bpyEA)(bpy)$_2$](CF$_3$CO$_2$)$_2$)$_{16}$) (**[Ru]@BCP4**), R^1 = 1,1-dimethyl-2-carboxyethyl, R^2 = SG1.

To a solution of 35.0 mg (0.43 µmol) **[Ru]@BCP2** in 0.2 mL of dry DCM slowly 254 mg (171 µL, 2.23 mmol) of TFA were added and stirred at 0 °C for 15 min. Subsequently, the mixture was stirred for 48 hours at room temperature. Afterwards the reaction mixture was diluted with 5 mL of DCM and purified by size exclusion chromatography (Biobeads SX-1, DCM). The orange colored, high molecular weight fraction was collected. Subsequently, all volatiles were removed under reduced pressure and the residue was dissolved in 1,4-dioxane prior to freeze-drying yielding an orange power as product. Yield: 26 mg. ^{1}H-NMR: (500.18 MHz, DMF-d$_7$, 297.0 K): δ [ppm] 8.98-8.76 (aromatic for [Ru]), 8.68-8.50 (aromatic for bpyEA), 8.40-8.27 (aromatic for bpyEA), 8.26-8.12 (aromatic for [Ru]), 8.06-7.94 (aromatic for [Ru]), 7.92-7.75 (aromatic for [Ru]), 7.67-7.50 (aromatic for [Ru]), 7.47-7.40 (aromatic for [Ru]), 7.35-6.37 (aromatic for styrene and bpyEA), 4.51-4.29 (C$_{ar}$-C*H*$_2$-CH$_2$O- for bpyEA and [Ru]), 2.58 (C$_{ar}$-C*H*$_3$ for [Ru]), 2.48-1.00 (C$_{ar}$-C*H*$_3$ for bpyEA, backbone).

Attachment of [Rh] to PS-*b*-P(*t*BuA-*co*-bpyEA-*co*-([Ru(bpy)$_2$(bpyEA)](PF$_6$)$_2$)

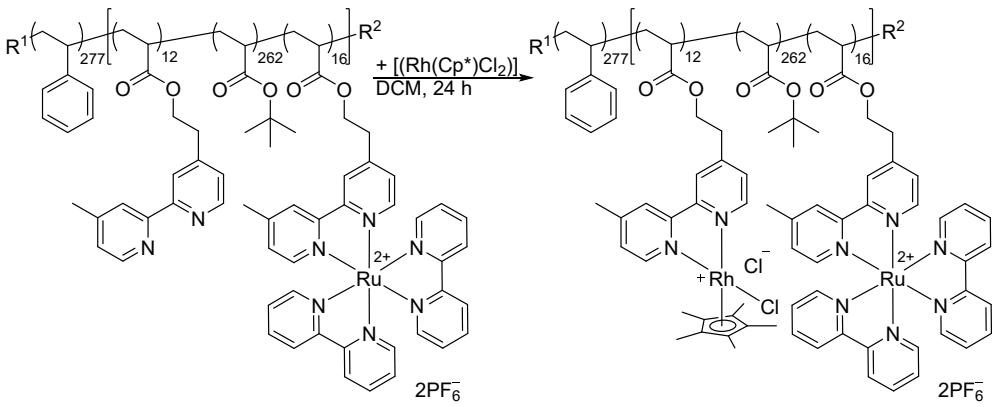

Scheme S8: Synthesis of PS$_{277}$-*b*-P(*t*BuA$_{262}$-*co*-([Rh(bpyEA)(Cp*)Cl]Cl)$_{12}$-*co*-([Ru(bpyEA)(bpy)$_2$]) (PF$_6$)$_2$)$_{16}$) (**[Rh]+[Ru]@BCP2**), R^1 = 1,1-dimethyl-2-carboxyethyl, R^2 = SG1.

A solution of 10.0 mg (0.120 µmol) **[Ru]@BCP4** block copolymer and 1.82 mg (2.94 µmol) of [Rh(Cp*)Cl$_2$]$_2$ in 0.5 mL DCM was stirred overnight at room temperature. Afterwards, the orange-

colored reaction mixture was purified by gel permeation chromatography (Biobeads SX-1, DCM). The high molecular orange colored fraction was collected and freed from all volatiles before being dissolved in 1,4-dioxane for freeze-drying. An orange powder was obtained as product. Yield: 10.5 mg. ^{1}H-NMR: (300.13 MHz, CD_2Cl_2, 300.0 K): δ [ppm] 8.86-8.24 (aromatic for [Ru] and [Rh]), 8.09 (aromatic for [Ru]), 7.86-7.36 (aromatic for [Ru] and [Rh]), 7.29-6.31 (aromatic for styrene, [Ru] and bpyEA), 4.54-4.17 (C_{ar}-CH_2-CH_2O- for [Ru] and [Rh]), 3.33-3.13 (C_{ar}-CH_2-CH_2O- for [Ru] and [Rh]), 2.68-2.49 (C_{ar}-CH_3 for [Ru] and [Rh]), 2.44-1.00 (backbone, 1.71 (-CH_3 for Cp*), 1.44 (-O-C(CH_3)$_3$ for ^{t}BuA).

PS-*b*-P(AA-*co*-([Rh(bpyEA)(Cp*)Cl]CF_3CO_2)-*co*-([Ru(bpy)$_2$(bpyEA)](CF_3CO_2)$_2$))

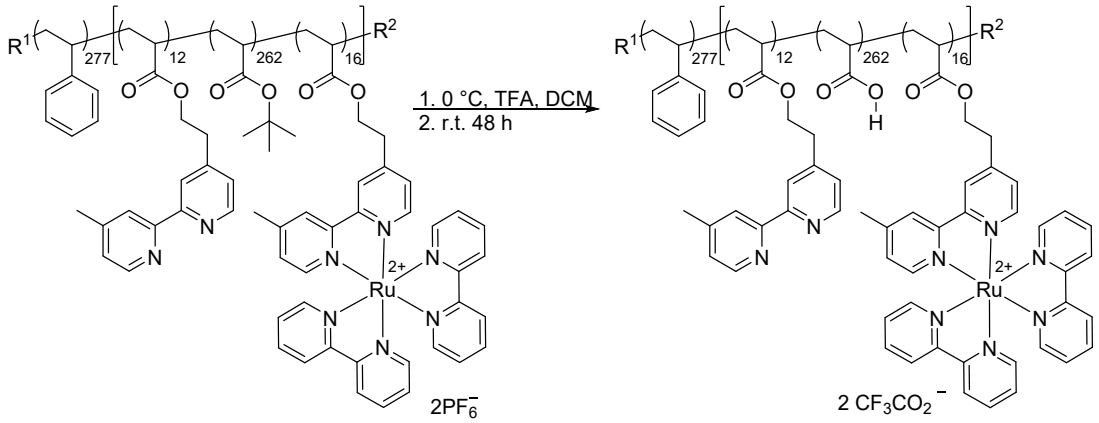

Scheme S9: Synthesis of PS_{277}-*b*-P(AA_{262}-*co*-bpyEA$_{12}$-*co*-([Ru(bpyEA)(bpy)$_2$](CF_3CO_2)$_2$)$_{16}$) (**[Rh]+[Ru]@BCP5**), R^1 = 1,1-dimethyl-2-carboxyethyl, R^2 = SG1.

To a solution of 7.0 mg (0.081 μmol) (**[Rh]+[Ru]@BCP2** in 0.5 mL of dry DCM slowly 48.6 mg (32.8 μL, 0.426 mmol) of TFA were added and stirred at 0 °C for 15 min. Subsequently, the mixture was stirred for 48 hours at room temperature. Afterwards the reaction mixture was diluted with 5 mL of DCM and purified by size exclusion chromatography (Biobeads SX-1, DCM). The orange colored, high molecular weight fraction was collected. Subsequently, all volatiles were removed under reduced pressure and the residue was dissolved in 1,4-dioxane prior to freeze-drying yielding an orange power as product. Yield: 5.0 mg.

S3 Micellization procedure

Samples with only one metal species

5 mg of block copolymer was dissolved in 2 mL of DMF. 2 mL of deionized water was added under stirring *via* a syringe pump (42 µL/min). The gradual decrease in solvent quality was observed by an increasing turbidity. Afterwards the mixture was stirred for one hour. After that time 6 mL of aqueous NH_3 solution (8 µM) in case of **[Ru]@BCP4** were added rapidly. For [Rh]-functionalized block copolymers 6 mL deionized water was added accordingly. The difference in procedures is reasoned by the following explanation. In contrast to [Rh]-functionalized block copolymers micellization of **[Ru]@BCP4** was carried out under slightly basic conditions. To prevent precipitation through intermicellar complexation the pH was kept at 9.5 during the micellization process. In detail, sufficient hydrophilicity in the second block is provided by deprotonated PAA units, whereas positively charged [Ru] moieties along with partially protonated bpyEA units lead to intermicellar complexation at slightly acidic conditions during the micellization process.

Sample containing both metal species

5 mg of block copolymer was suspended in 2 mL of DMF and dropwise TFA was added. Until no visible turbidity was observed. Deionized water was added *via* a syringe pump (42 µL/min) until noticeable turbidity. 6.65 M of aqueous NH_3 solution was added until reaching a pH of 9.5. Directly afterwards the addition of deionized water under stirring *via* a syringe pump (42 µL/min) was continued until reaching 50:50 volume ratio of DMF/water. The mixture was stirred for one hour and subsequently 6 mL of deionized water was added. For [Rh] containing block copolymers deionized water, and for the preparation of [Ru] micelles an aqueous NH_3 solution at pH 9.5 as selective solvent was utilized. However, for the both [Rh] and [Ru]-containing sample deionized water was used to induce micellization in a first step (acidic regime). Initial acidic conditions are induced by TFA so solubilize the block copolymer in the first place. Concentrated NH_3 solution was added afterwards to shift pH from strongly acidic to 9.5 without excessively increasing water content during pH change. In the last step of micellization again deionized water was added maintaining a pH of 9.5 prior to dialysis.

Further purification

Regardless of the sample, stirring was continued overnight. Subsequently, the micellar solution was dialyzed against deionized water (MWCO 12-14 kDA) for at least 4 days with minimum 8 changes of the dialysis water.

S4 Catalysis

All catalysis experiments were performed under argon atmosphere inside screw-cap sealed air-tight quartz glass cuvettes with 10 mm path length. The total volume for each catalysis experiment was V = 2.50 mL. Heating of the samples was performed using a water bath. All sample preparation steps – except the addition of molecular model complexes to the GC vials, used for mixing of all components prior to the transfer of the final solution to the cuvettes, i.e. [Rh(dmbpy)(Cp*)Cl]Cl or $[Ru(bpy)_3]Cl_2$ x $6H_2O$ *via* stock solution and subsequent evaporation of the stock solution solvent – were performed in an Ar-filled glovebox. The Ru and Rh concentration was always 5 µM, irrespective whether the polymeric or the molecular material was investigated. In all cases de-ionized water was used as solvent which has been thoroughly degassed by bubbling Ar through the liquid prior to its introduction into the Ar-filled glovebox.

Catalytic turnover was monitored in defined time intervals using UV/vis absorption as well as emission spectroscopy (λ_{exc} = 340 nm). For UV/vis-spectroscopic investigation a JASCO V-670 UV-vis-NIR spectrometer and for emission spectroscopy a JASCO FP-8500 fluorescence spectrometer was used.

Sample preparation.

For the light-independent NAD^+ reduction experiments using sodium formate as reducing agent the samples were prepared as follows: To the GC-vial already eventually containing either [Rh(dmpby)(Cp*)Cl]Cl or $[Ru(bpy)_3]Cl_2$ x $6H_2O$ (depending whether one of these compounds was planned to be part of the catalytic mixture) initially 1.00 mL of a 125 mM aqueous $NaHCO_2$ solution (final concentration: 50 mM) were added, followed by the addition of 0.50 mL of a 1.25 mM aqueous NAD^+ solution (final concentration: 250 µM). The remaining 1 mL of solvent was either pure deionized water if no micellar material was planned to be part of the catalytic solution or a mixture of an appropriate amount of an aqueous micellar suspension to yield 5 µM Rh or Ru and deionized water. After shaking the GC-vial to ensure homogeneous mixing of all components, the catalytic solution was transferred to the quartz glass cuvettes and sealed with a screw-cap. After taking the cuvettes out of the Ar-filed glovebox, "0 min"-measurements (UV/vis absorption and emission spectroscopy) were performed before the samples were further allowed to stay at room temperature or were placed in the water bath if the catalysis was planned to be investigated at elevated temperatures.

For the light-dependent NAD^+ reduction experiments using triethylamine (TEA) as reducing agent the samples were prepared as follows: Sample preparation was identical to what was described above for the light-independent process, except that in the beginning 1 mL of an aqueous buffer system containing 0.30 M TEA and 0.25 M NaH_2PO_4 (final concentration: 0.12 M TEA, 0.1 M NaH_2PO_4) instead of the sodium formate solution was added. After removing the cuvettes from the Ar-filled glovebox, a "0 min"-measurements was performed before the samples were placed in a custom-made air-cooling apparatus

equipped with one blue light emitting LED-stick (λ_{max} = 463 nm, 45-50 mW/cm^2) that has been described previously.[4]

Data interpretation: For determining the catalytic activity as well as the selectivity of the overall process, samples of known concentrations of commercially available pure NADH (Merck) in deionized water were analyzed by UV/vis and emission spectroscopy under the same conditions as the catalytic mixtures. The signal response during catalysis was compared to the signal intensities received from measurements of known concentrations of commercially available NADH, finally yielding turnover number (TON), turnover frequency (TOF) and selectivity of the catalyst system.

S5 Supplementary figures and tables

NMR spectra

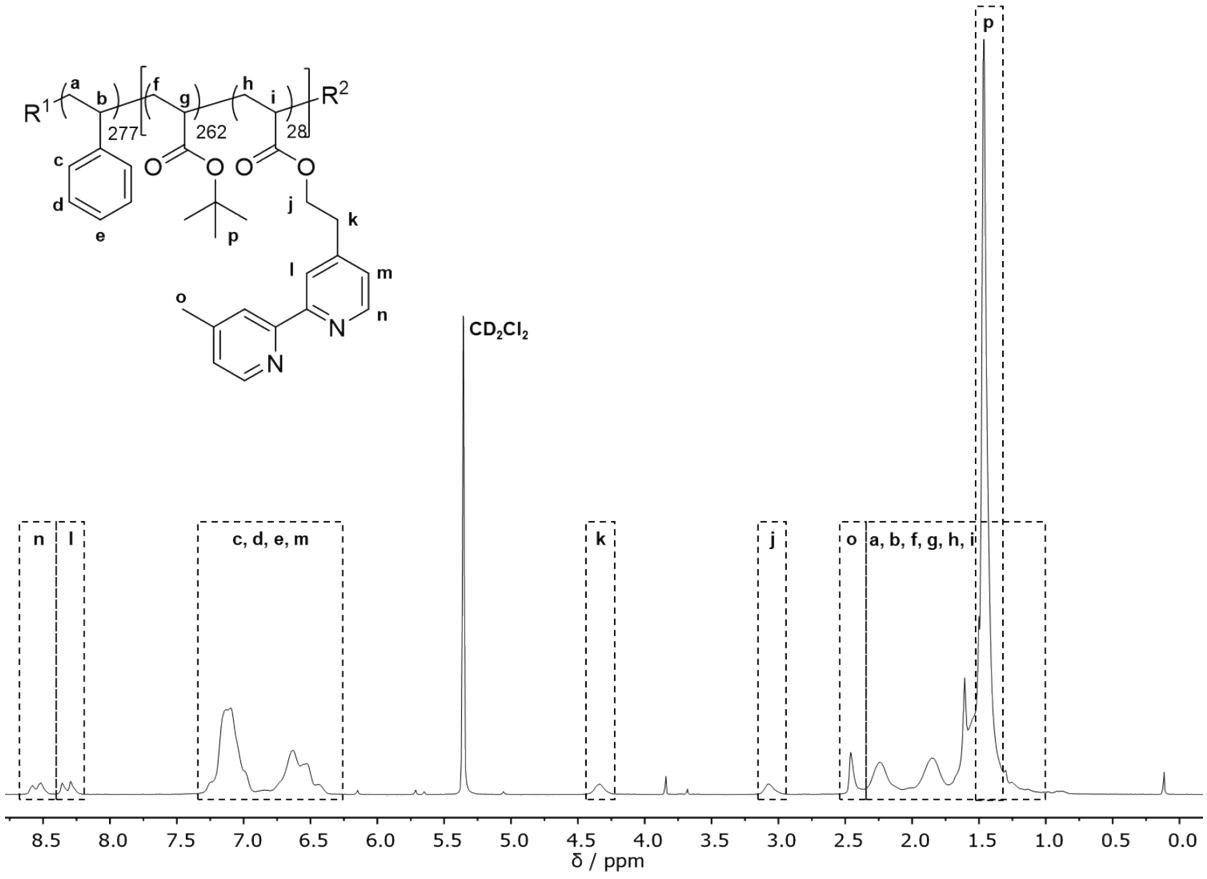

Figure S1: ^{1}H-NMR spectrum of PS_{277}-*b*-P(^{t}BuA$_{262}$-*co*-bpyEA$_{28}$) (**BCP2**) (300.13 MHz, CD_2Cl_2, 300.0 K) and signal assignment, R^1 = 1,1-dimethyl-2-carboxyethyl, R^2 = SG1.

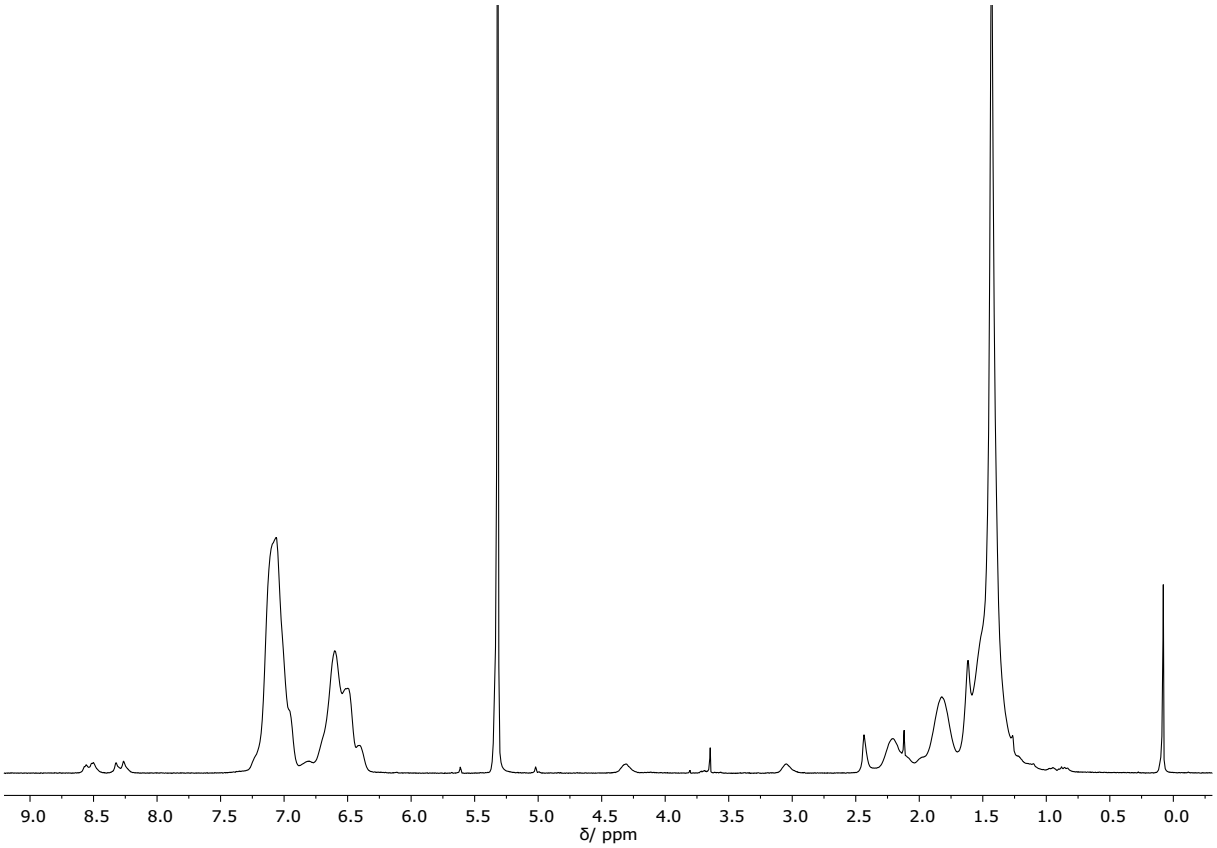

Figure S2: ^{1}H-NMR spectrum of PS_{277}-*b*-P(^{t}BuA_{99}-*co*-bpyEA_{9}) (**BCP1**) (300.13 MHz, CD_2Cl_2, 300.0 K).

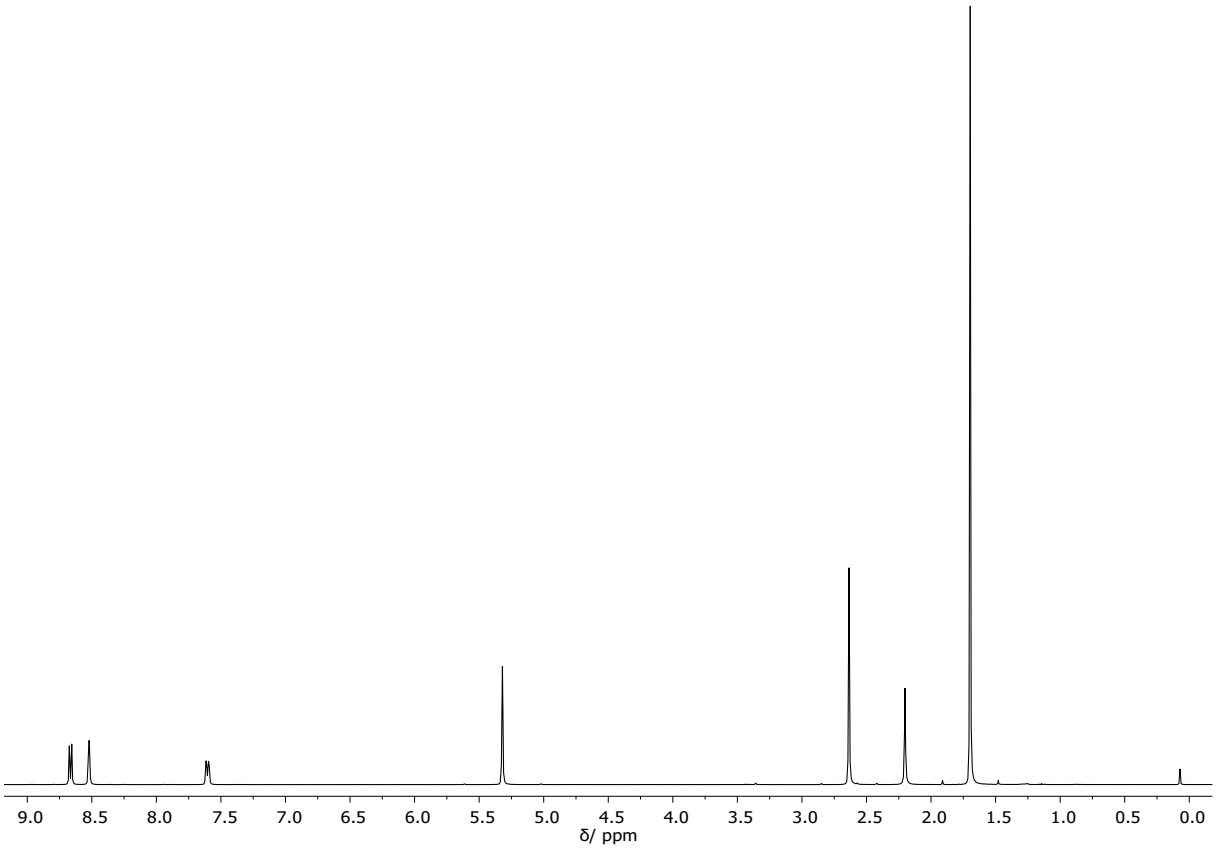

Figure S3: ^{1}H-NMR spectrum of [Rh(dmbpy)(Cp*)Cl]Cl (**1**) (300.13 MHz, CD_2Cl_2, 300.0 K).

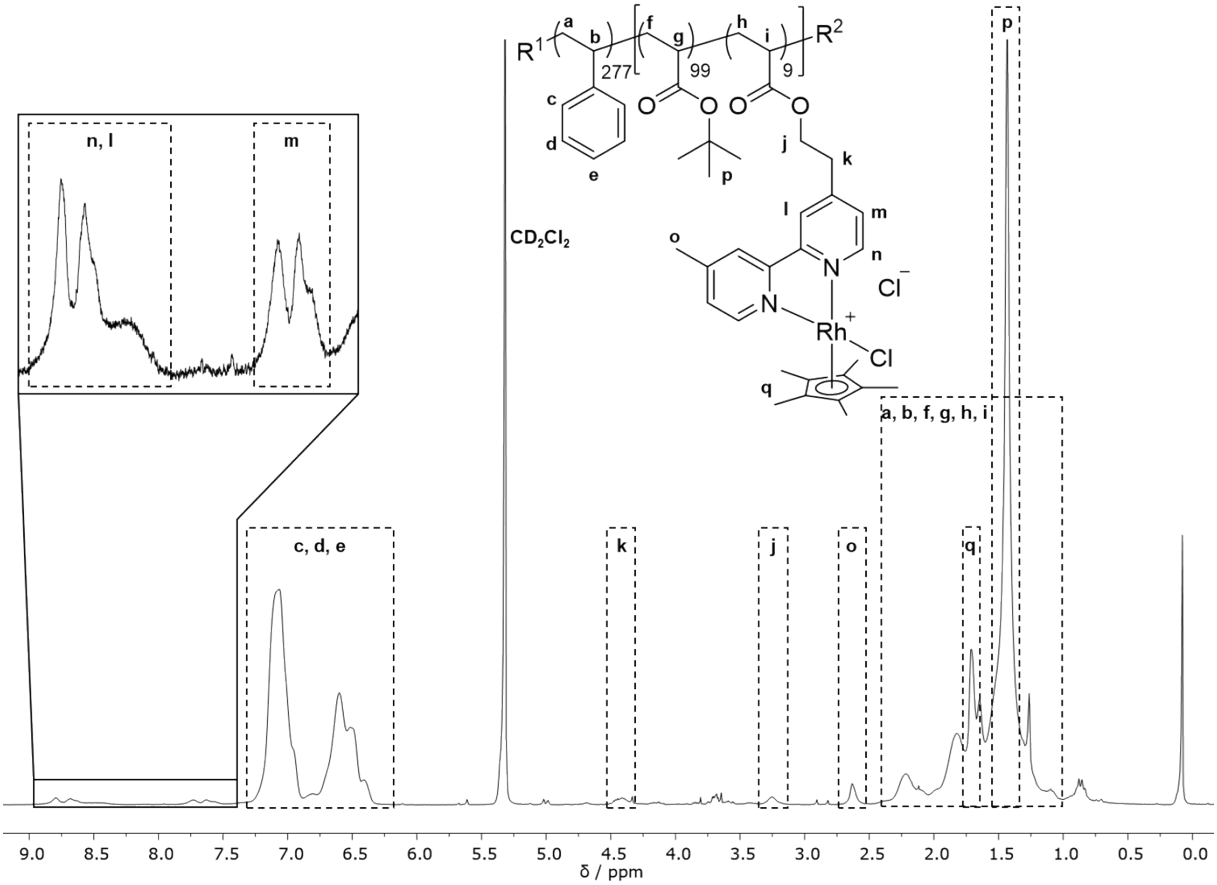

Figure S4: ^{1}H-NMR spectrum of PS_{277}-*b*-P(^{t}BuA_{99}-*co*-([Rh(bpyEA)(Cp*)Cl]Cl)$_9$) (**[Rh]@BCP1**) (300.13 MHz, CD_2Cl_2, 300.0 K) and signal assignment, R^1 = 1,1-dimethyl-2-carboxyethyl, R^2 = SG1.

By comparing the integrals for signals **n**, **l** and **m** with **c, d** and **e** the degree of functionalization (DoF) was calculated to >99 % of bpyEA units are functionalized with [Rh].

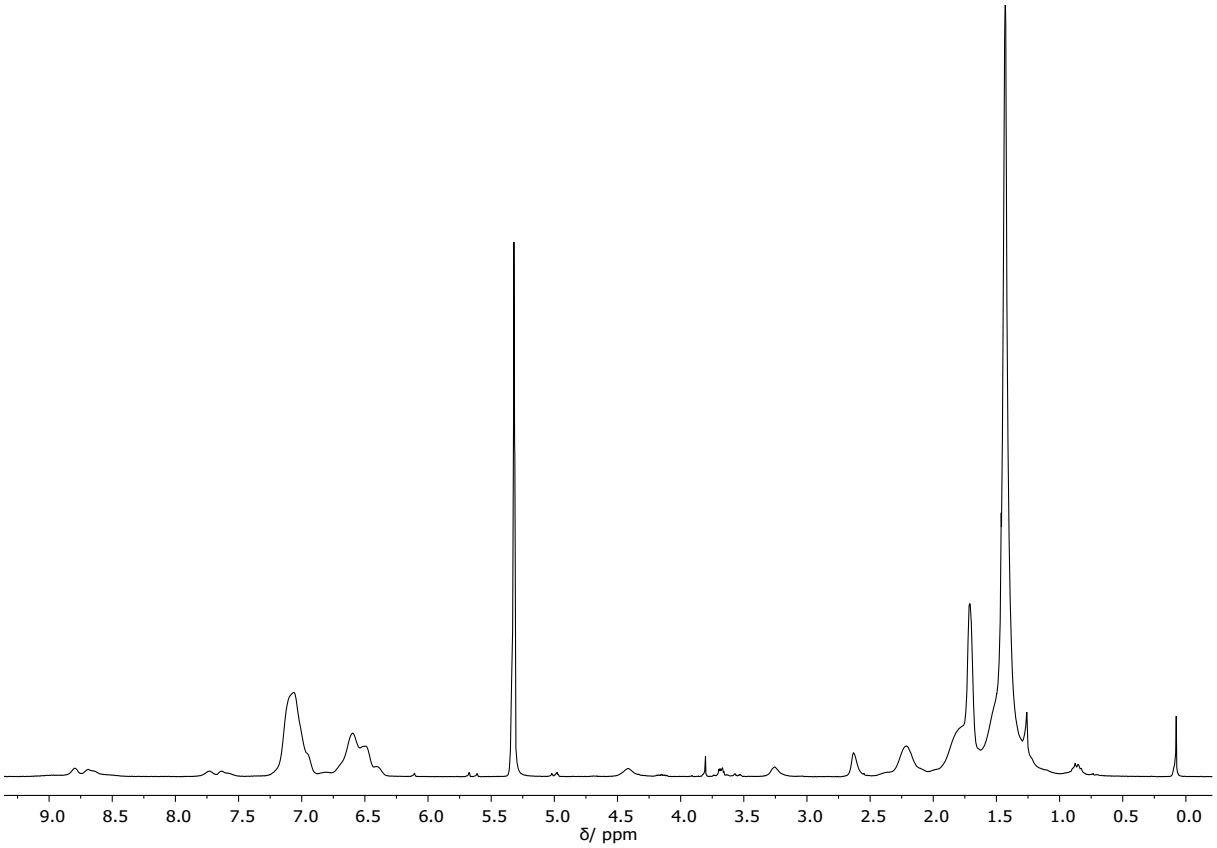

Figure S5: ^{1}H-NMR spectrum of PS_{277}-*b*-P(^{t}BuA_{262}-*co*-([Rh(bpyEA)(Cp*)Cl]Cl)$_{28}$) (**[Rh]@BCP2**) (300.13 MHz, CD_2Cl_2, 300.0 K).

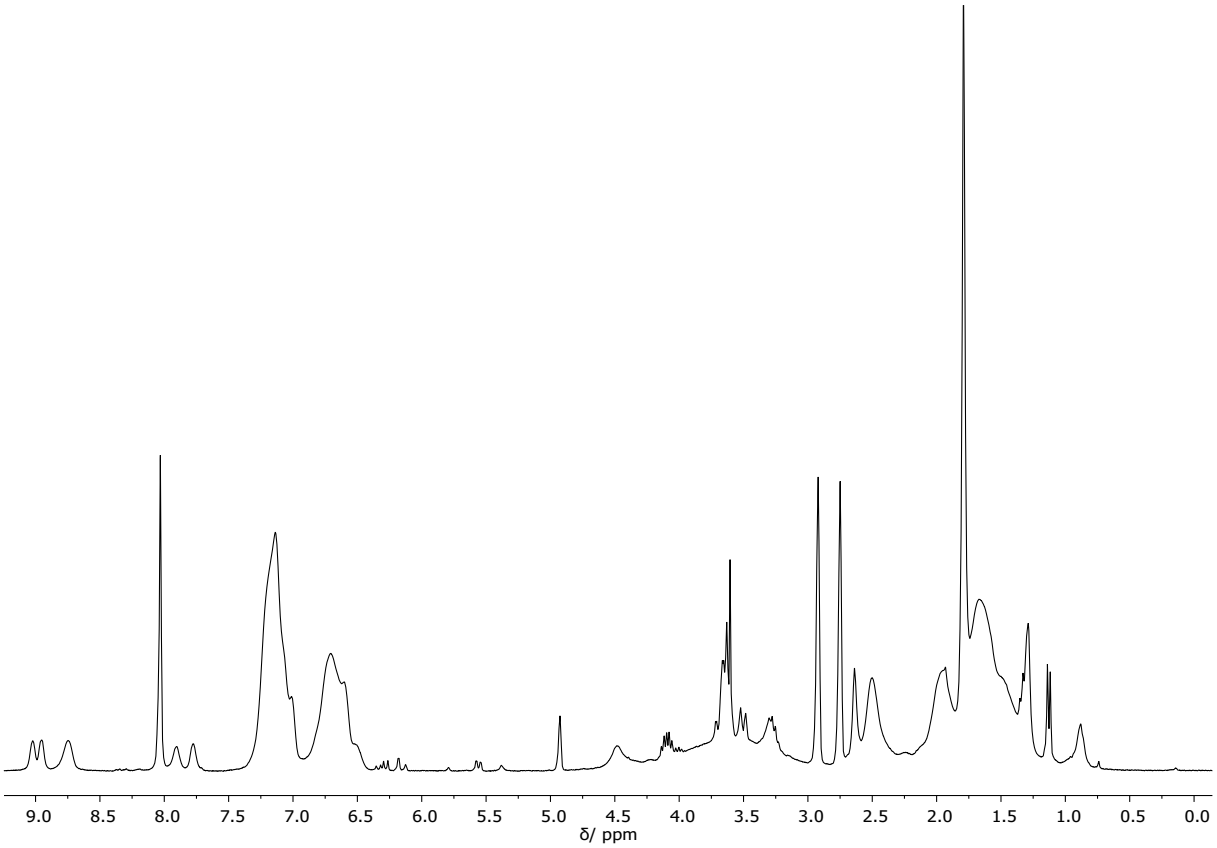

Figure S6: ^{1}H-NMR spectrum of PS_{277}-*b*-P(AA_{262}-*co*-([Rh(bpyEA)(Cp*)Cl]CF_3CO_2)$_{28}$) (**[Rh]@BCP4**) (300.13 MHz, DMF-d_7, 300.0 K).

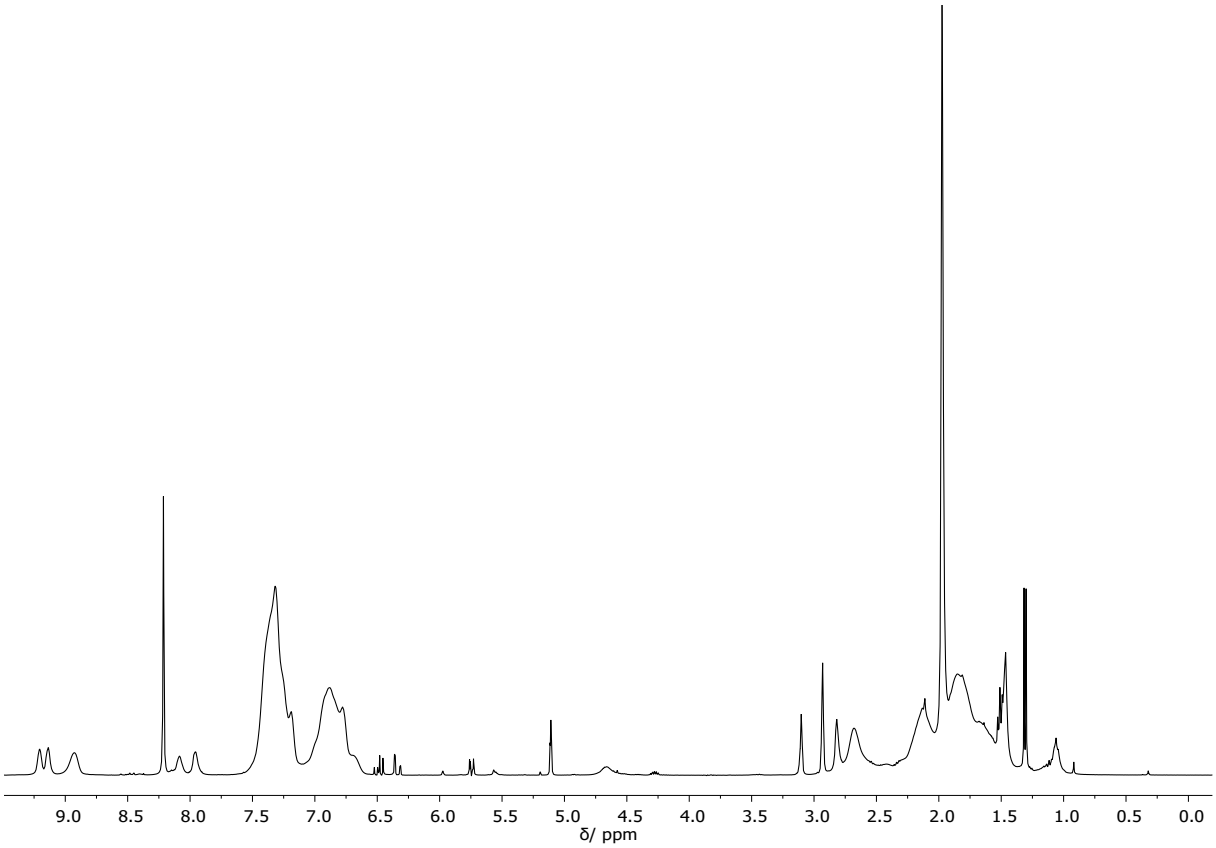

Figure S7: ^{1}H-NMR spectrum of PS_{277}-*b*-P(AA_{262}-*co*-([Rh(bpyEA)(Cp*)Cl]CF_3CO_2)$_{28}$) (**[Rh]@BCP4**) (300.13 MHz, DMF-d_7, 300.0 K), water signal suppression.

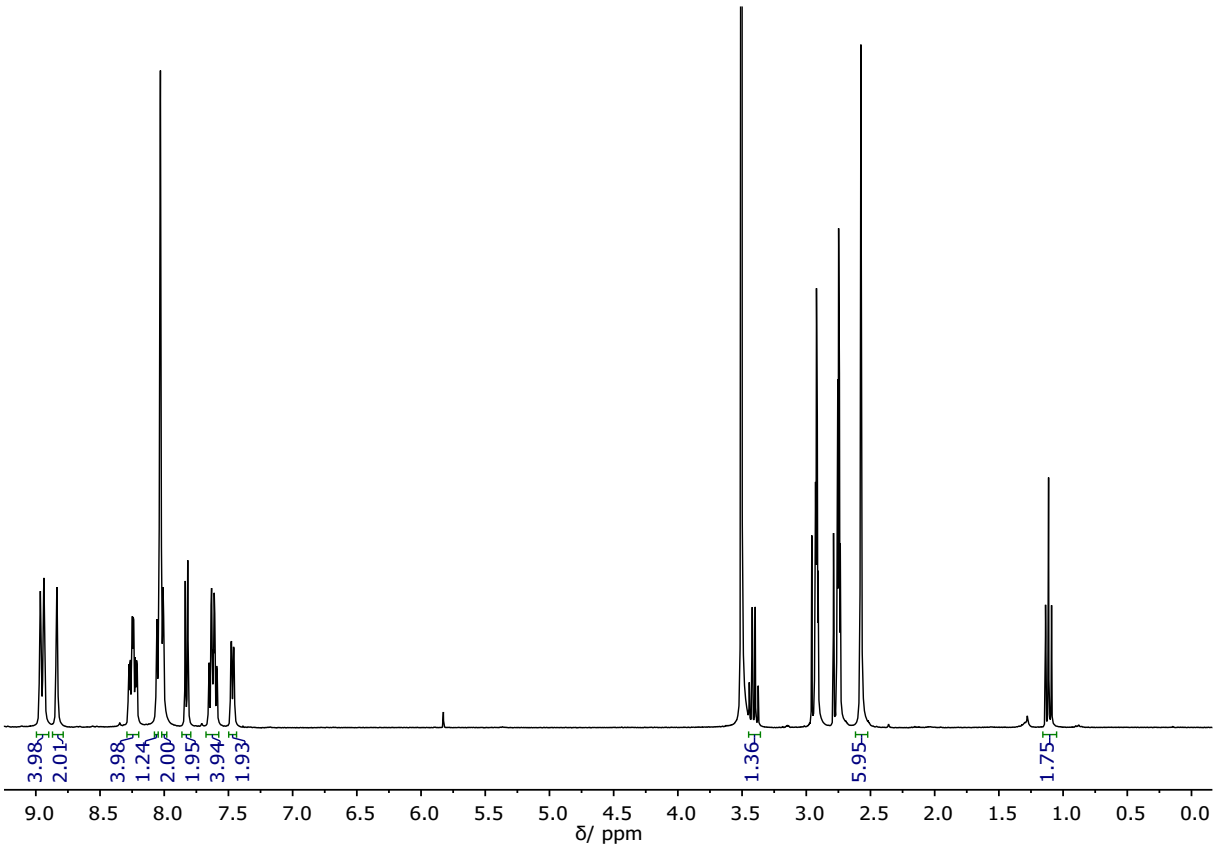

Figure S8: ^{1}H-NMR spectrum and signal integration of [Ru(bpy)$_2$(dmbpy)](PF$_6$)$_2$ (300.13 MHz, DMF-d_7, 300.0 K).

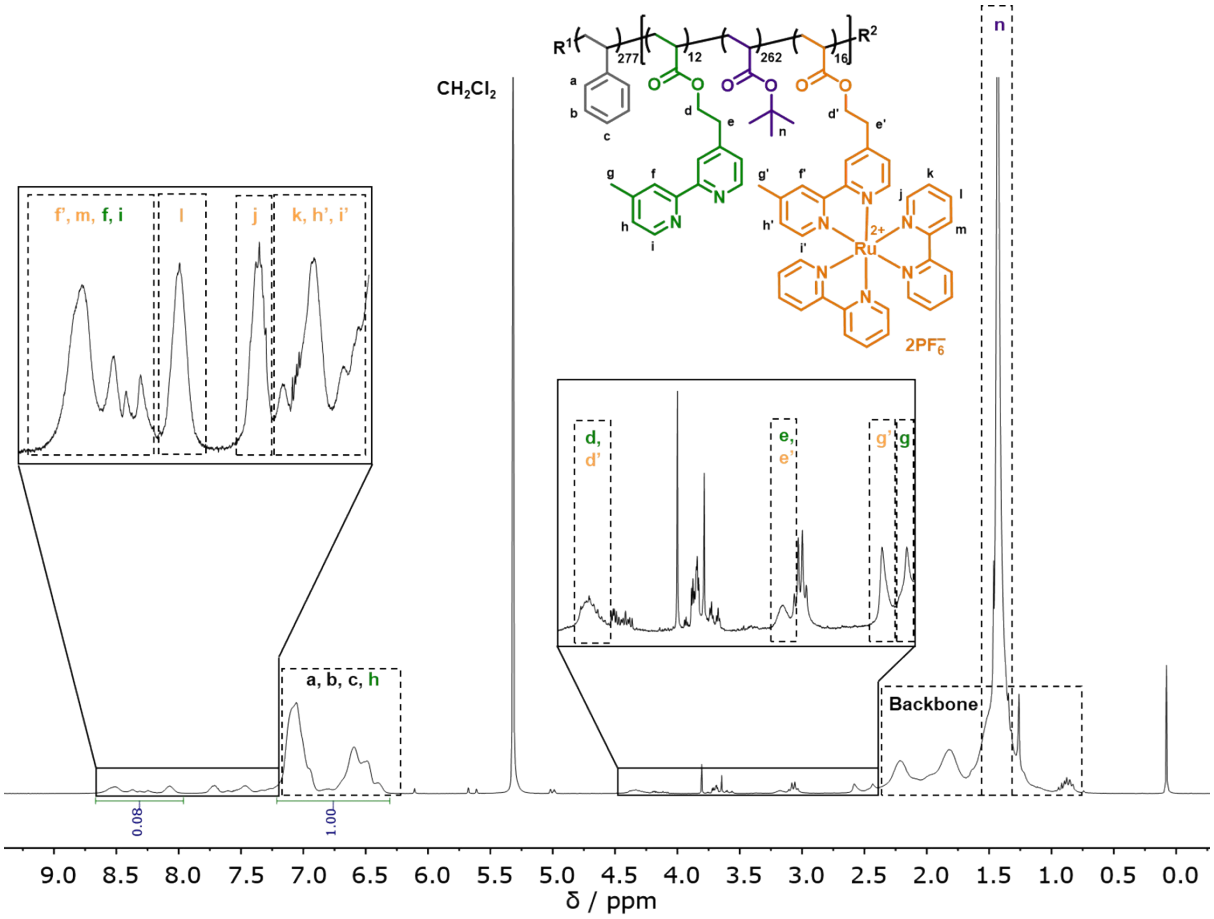

Figure S9: ^{1}H-NMR spectrum of PS_{277}-*b*-P(^{t}BuA_{262}-*co*-bpyEA_{12}-*co*-([Ru(bpyEA)(bpy)$_2$](PF_6)$_2$)$_{16}$) (**[Ru]@BCP2**) in CD_2Cl_2 and signal assignment.

By comparing the integrals for signals **f'**, **m**, **f** and **i** with **l** the degree of functionalization (DoF) was calculated to 57 % of bpyEA units are functionalized with [Ru].

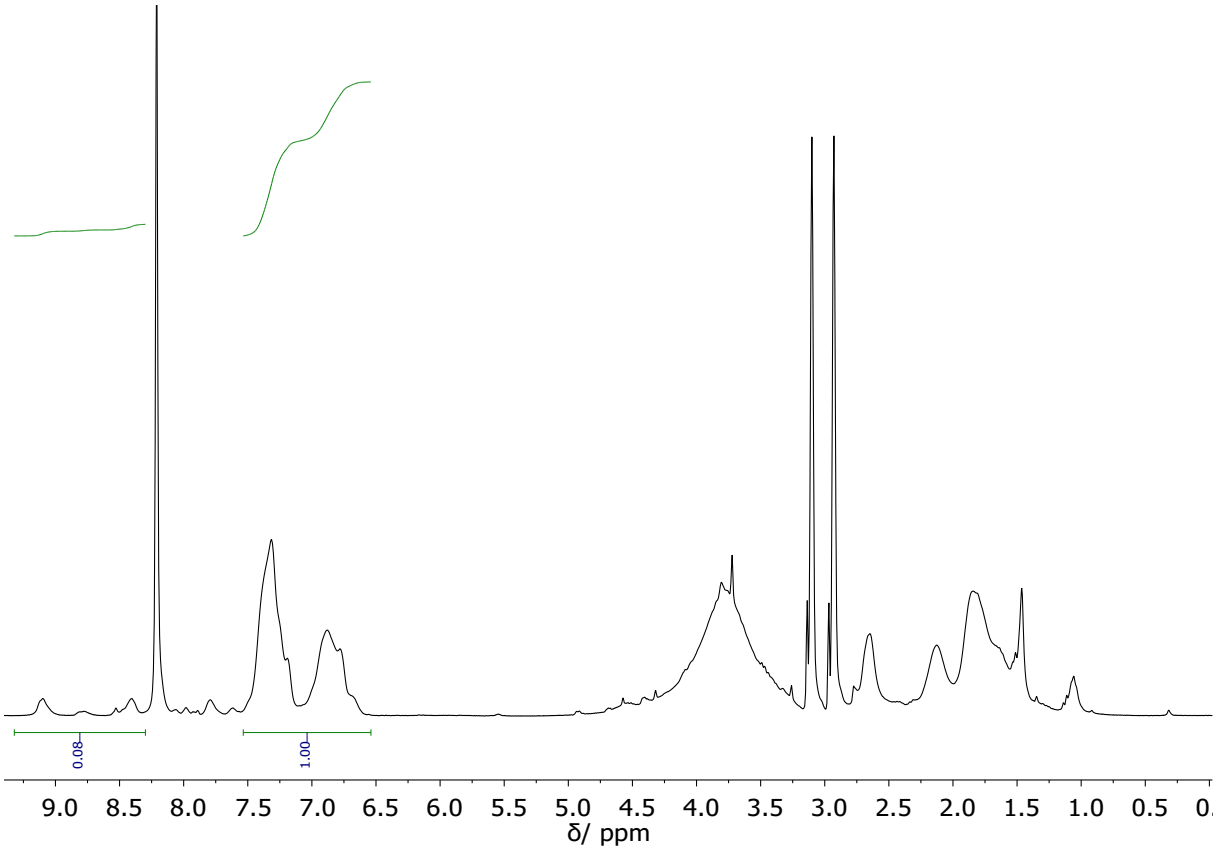

Figure S10: ^{1}H-NMR spectrum of PS_{277}-*b*-P(AA_{262}-*co*-$bpyEA_{12}$-*co*-([Ru(bpyEA)(bpy)$_2$](CF_3CO_2)$_2$)$_{16}$) (**[Ru]@BCP4**) (300.13 MHz, DMF-d_7, 300.0 K).

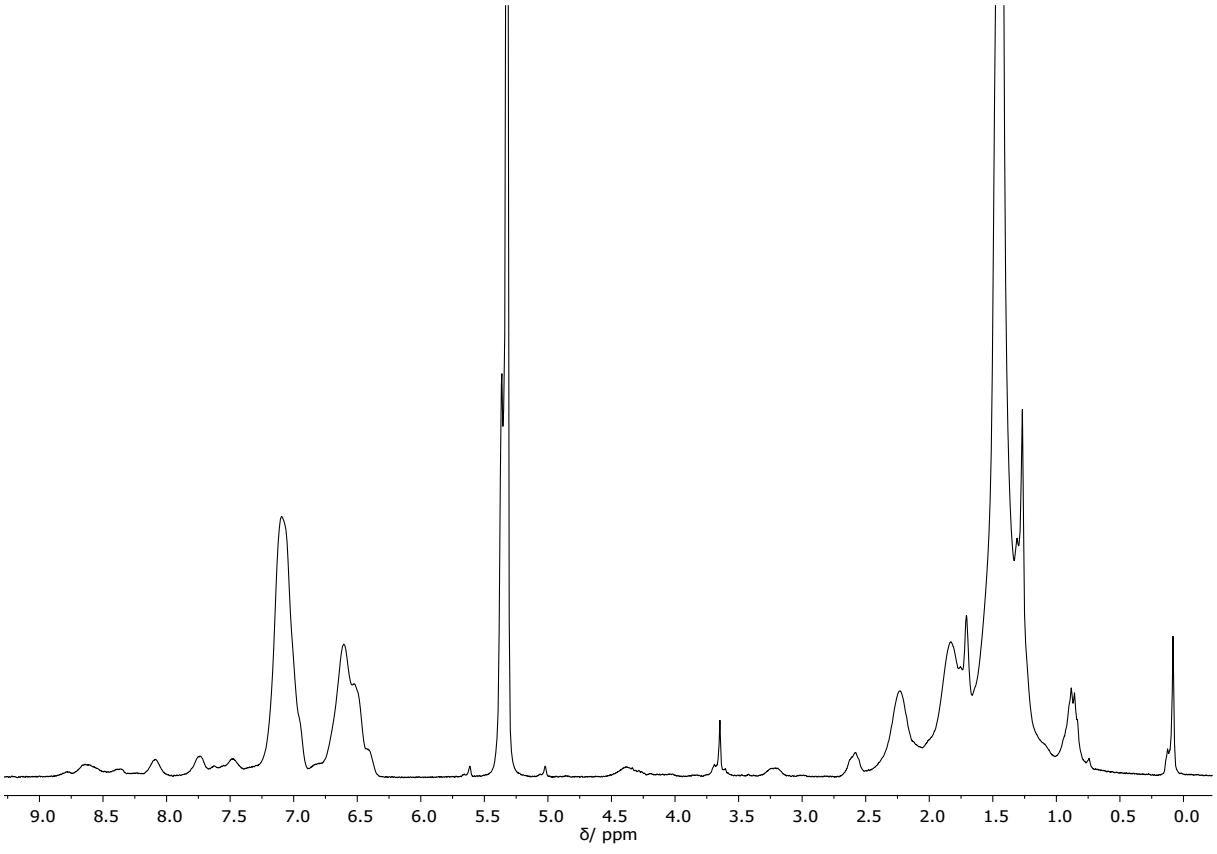

Figure S11: ^{1}H-NMR spectrum of PS_{277}-*b*-P($^{t}BuA_{262}$-*co*-([Rh(bpyEA)(Cp*)Cl]Cl)$_{12}$-*co*-([Ru(bpyEA)(bpy)$_2$]) (PF_6)$_2$)$_{16}$) (**[Rh]+[Ru]@BCP2**) (300.13 MHz, CD_2Cl_2, 300.0 K).

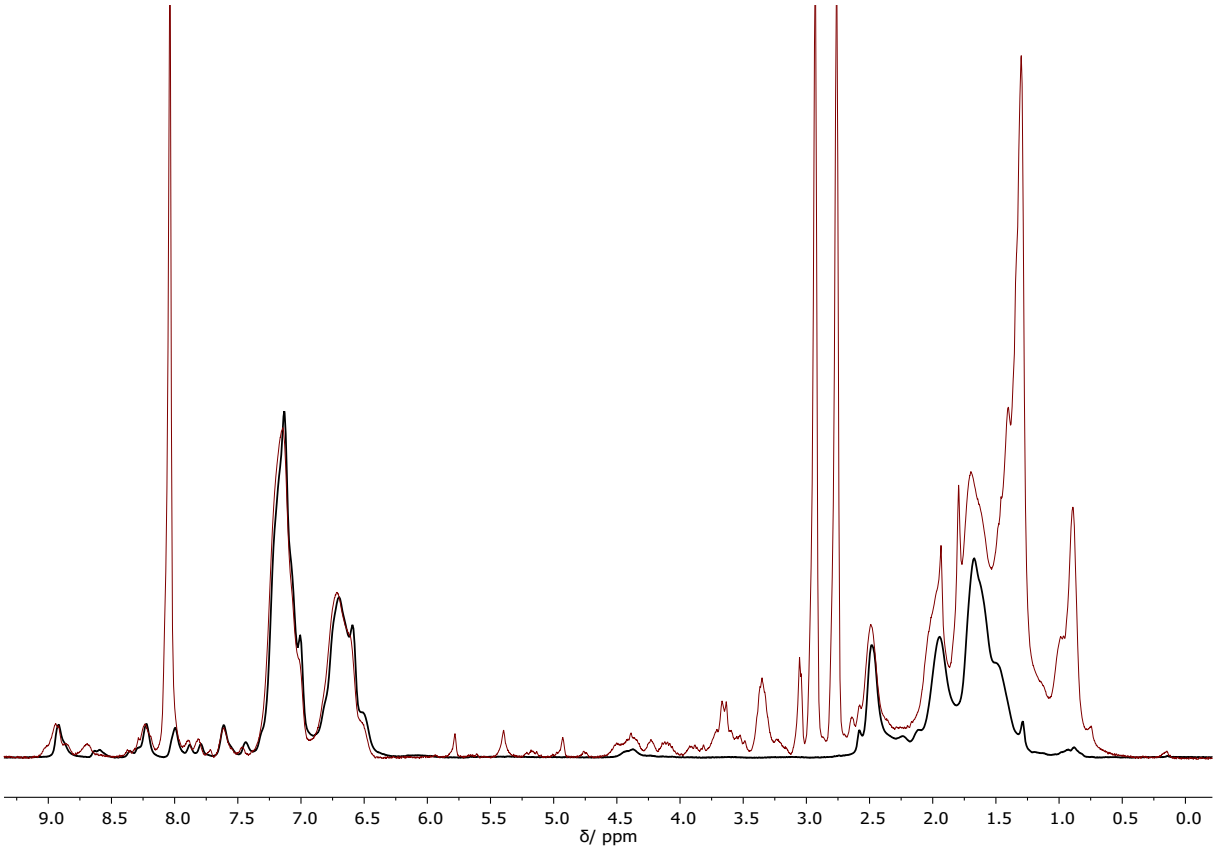

Figure S12: Overlay of ^{1}H-NMR spectrum of **[Ru]@BCP4** (black line, water- and solvent signal suppression, 500.18 MHz, DMF-d_7, 297.0 K) and **[Rh]+[Ru]@BCP5** (red line, 300.13 MHz, DMF-d_7 + TFA, 300.0 K).

SEC data and UV/vis spectra

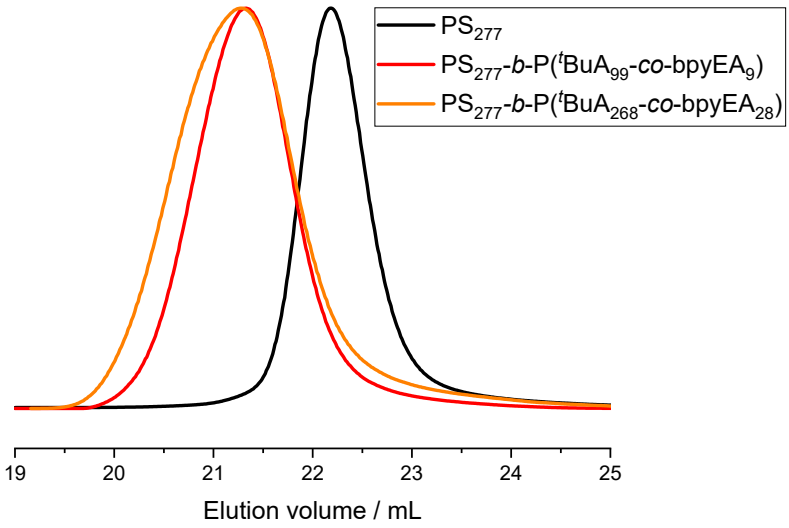

Figure S13: Normalized RI SEC elution traces of PS_{277}, PS_{277}-*b*-P(^{t}BuA$_{99}$-*co*-bpyEA$_9$) (**BCP1**) and PS_{277}-*b*-P(^{t}BuA$_{262}$-*co*-bpyEA$_{28}$) (**BCP2**).

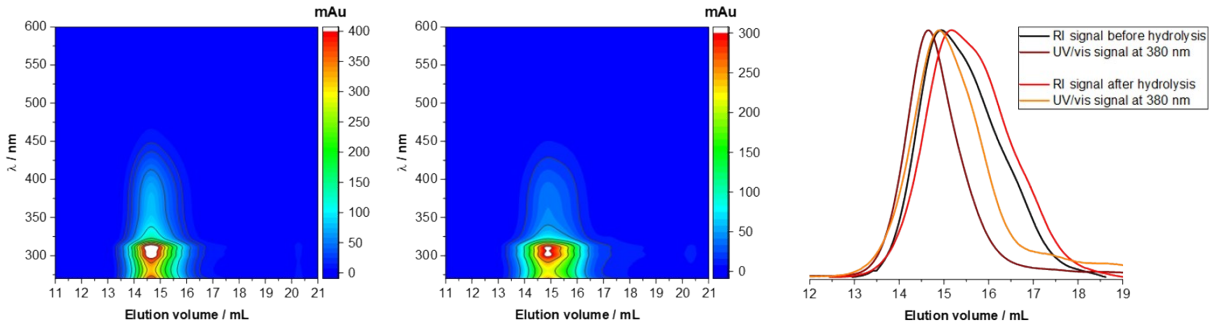

Figure S14: SEC-coupled in-line diode array spectra for PS_{277}-*b*-P(^{t}BuA$_{262}$-*co*-([Rh(bpyEA)(Cp*)Cl]Cl)$_{28}$) (**[Rh]@BCP2**) (left) and PS_{277}-*b*-P(AA_{262}-*co*-([Rh(bpyEA)(Cp*)Cl]CF_3CO_2)$_{28}$) (**[Rh]@BCP4**) (middle); RI elution traces and UV/vis absorption traces before and after deprotection of ^{t}BuA units (right).

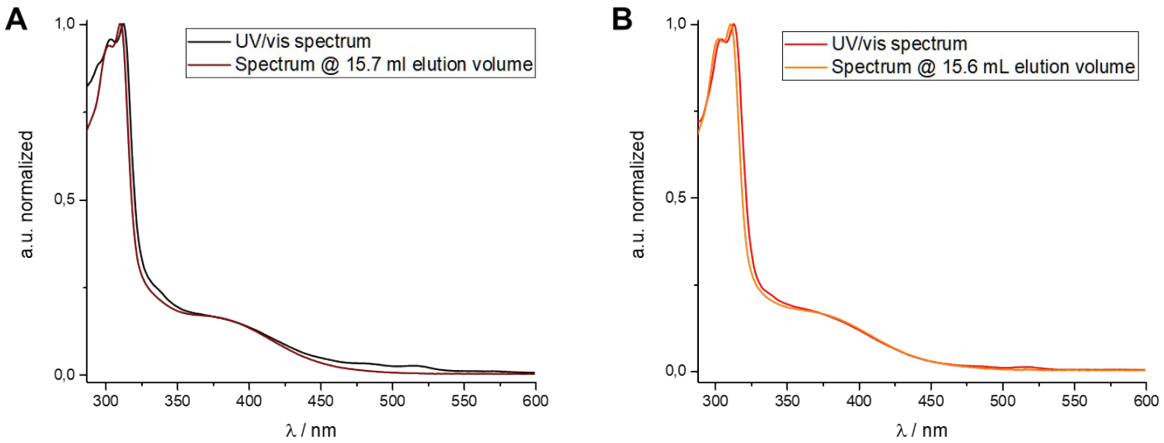

Figure S15: **A**: Black: UV/vis spectra of PS_{277}-*b*-P(^{t}BuA$_{99}$-*co*-([Rh(bpyEA)(Cp*)Cl]Cl)$_9$) (**[Rh]@BCP1**) in DMAC + 0.08 wt.% NH_4PF_6, c = 160 mg/L, a.u. (arbitrary unit), normalized; Brown: diode array spectrum of **[Rh]@BCP1** from in-line SEC analysis, elution volume = 15.7 mL, normalized. **B**: Red: UV/vis spectra of PS_{277}-*b*-P(AA_{99}-*co*-([Rh(bpyEA)(Cp*)Cl] CF_3CO_2)$_9$) (**[Rh]@BCP3**) in DMAC + 0.08 wt.% NH_4PF_6, c = 160 mg/L, normalized; Orange: diode array spectrum of **[Rh]@BCP3** from in-line SEC analysis, elution volume = 15.6 mL, a.u. (arbitrary unit), normalized.

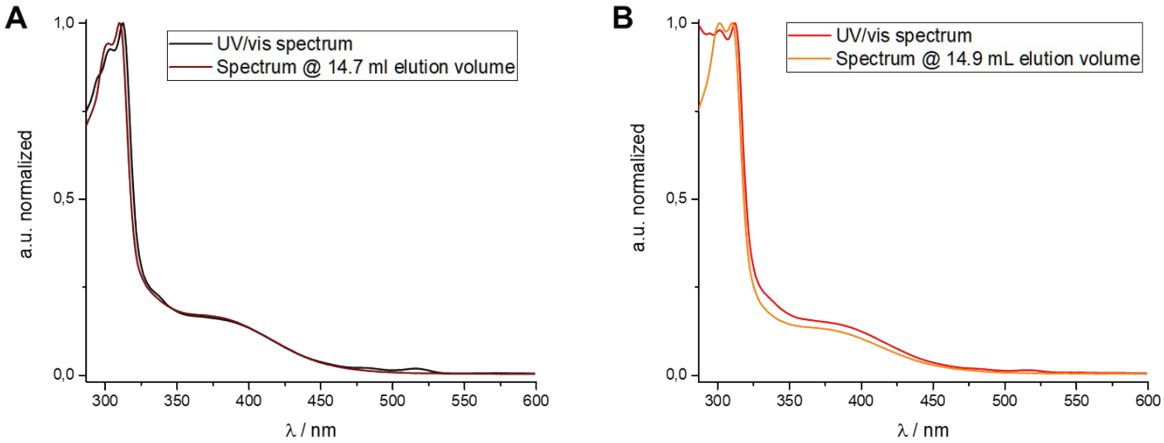

Figure S16: **A**: Black: UV/vis spectra of PS_{277}-*b*-P(^{t}BuA$_{262}$-*co*-([Rh(bpyEA)(Cp*)Cl]Cl)$_{28}$) (**[Rh]@BCP2)** in DMAC + 0.08 wt.% NH_4PF_6, c = 160 mg/L, a.u. (arbitrary unit), normalized; Brown: diode array spectrum of **[Rh]@BCP2** from in-line SEC analysis, elution volume = 14.7 mL, normalized. **B**: Red: UV/vis spectra of PS_{277}-*b*-P(AA_{262}-*co*-([Rh(bpyEA)(Cp*)Cl] CF_3CO_2)$_{28}$) (**[Rh]@BCP4**) in DMAC + 0.08 wt.% NH_4PF_6, c = 160 mg/L, normalized; Orange: diode array spectrum of **[Rh]@BCP4** from in-line SEC analysis, elution volume = 14.9 mL, a.u. (arbitrary unit), normalized.

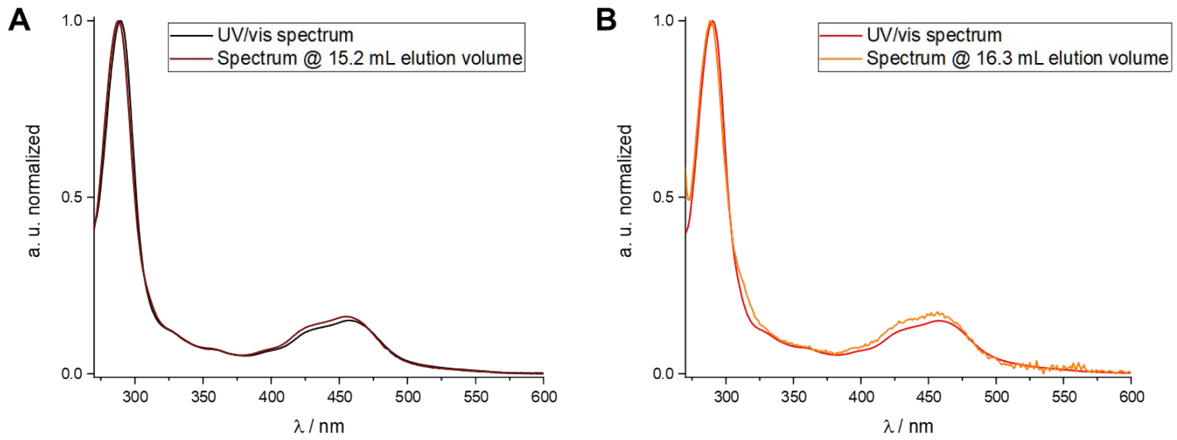

Figure S17: **A**: Black: UV/vis spectra of PS_{277}-*b*-P(^{t}BuA_{262}-*co*-bpyEA_{12}-*co*-([Ru(bpyEA)(bpy)$_2$](PF_6)$_2$)$_{16}$) (**[Ru]@BCP2**) in DMAC + 0.08 wt.% NH_4PF_6, c = 80 mg/L, normalized; Brown: diode array spectrum of **[Ru]@BCP2** from in-line SEC analysis, elution volume = 15.2 mL, a.u. (arbitrary unit), normalized. **B**: Red: UV/vis spectra of PS_{277}-*b*-P(AA_{262}-*co*-bpyEA_{12}-*co*-([Ru(bpyEA)(bpy)$_2$](CF_3CO_2)$_2$)$_{16}$) (**[Ru]@BCP4**) in DMAC + 0.08 wt.% NH_4PF_6, c = 80 mg/L, normalized; Orange: diode array spectrum of **[Ru]@BCP4** from in-line SEC analysis, elution volume = 16.3 mL, a.u. (arbitrary unit), normalized.

XPS analysis

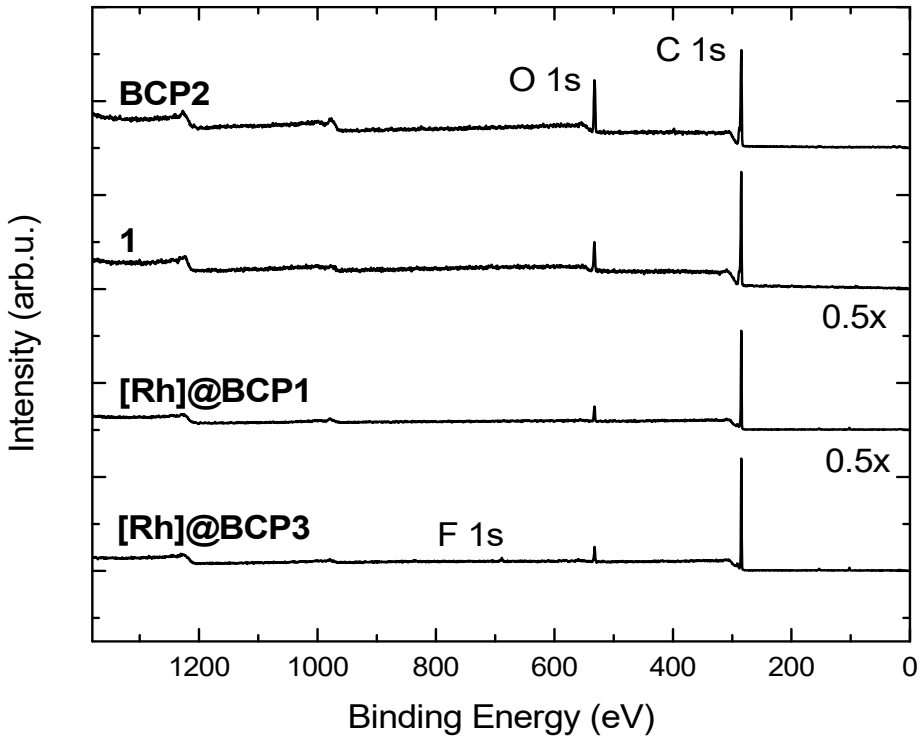

Figure S18: XP overview spectra of PS_{277}-*b*-P(^{t}BuA_{262}-*co*-bpyEA_{28}) (**BCP2**), [Rh(dmbpy)(Cp*)Cl]Cl (**1**), PS_{277}-*b*-P(^{t}BuA_{99}-*co*-([Rh(bpyEA)(Cp*)Cl]Cl)$_9$) (**[Rh]@BCP1**) and PS_{277}-*b*-P(AA_{99}-*co*-([Rh(bpyEA)(Cp*)Cl]CF_3CO_2)$_9$) (**[Rh]@BCP3**) after drop casting on Au/Si samples. For better representation, intensities of the spectra are multiplied by a factor given in the figure with respect to (**BCP2** and **1**).

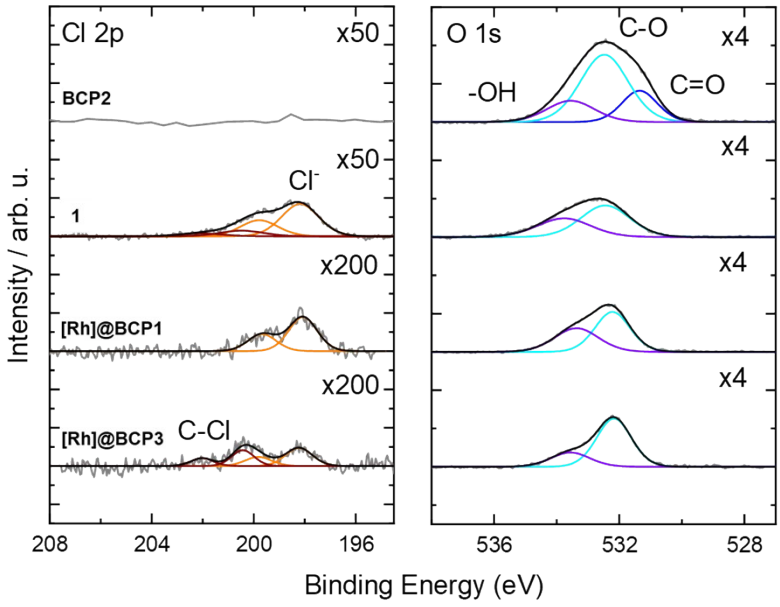

Figure S19: High resolution Cl 2p (left) and O 1s (right) XP spectra of PS_{277}-*b*-P(^{t}BuA_{262}-*co*-bpyEA_{28}) (**BCP2**), [Rh(dmbpy)(Cp*)Cl]Cl (**1**), PS_{277}-*b*-P(^{t}BuA_{99}-*co*-([Rh(bpyEA)(Cp*)Cl]Cl)$_9$) (**[Rh]@BCP1**) and PS_{277}-*b*-P(AA_{99}-*co*-([Rh(bpyEA)(Cp*)Cl]CF_3CO_2)$_9$) (**[Rh]@BCP3**). For better representation, intensities of the spectra are multiplied by a factor given in the figure with respect to the C 1s spectrum in Figure 2 of the main paper.

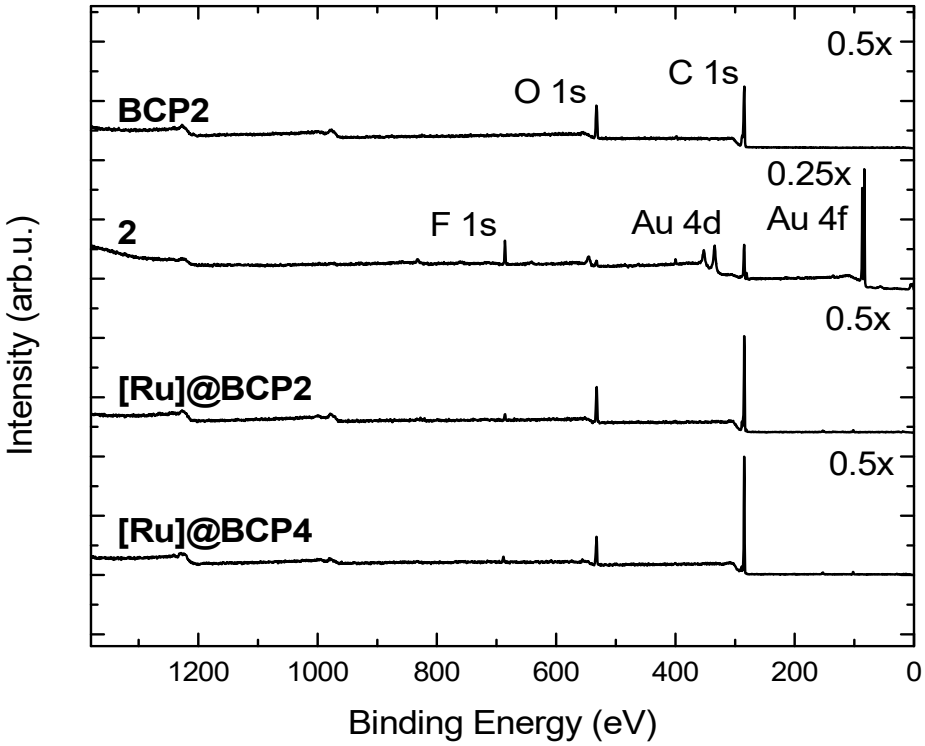

Figure S20: XP overview spectra of PS_{277}-*b*-P(^{t}BuA_{262}-*co*-bpyEA_{28}) (**BCP2**), [Ru(bpy)$_2$(dmbpy)](PF$_6$)$_2$ (**2**), PS_{277}-*b*-P(^{t}BuA_{262}-*co*-bpyEA_{12}-*co*-([Ru(bpyEA)(bpy)$_2$](PF$_6$)$_2$)$_{16}$) (**[Ru]@BCP2**) and PS_{277}-*b*-P(AA_{262}-*co*-bpyEA_{12}-*co*-([Ru(bpyEA)(bpy)$_2$](CF$_3$CO$_2$)$_2$)$_{16}$) (**[Ru]@BCP4**) after drop casting on Au/Si samples. For better representation, intensities of the spectra are multiplied by a factor given in the figure with respect to **2**.

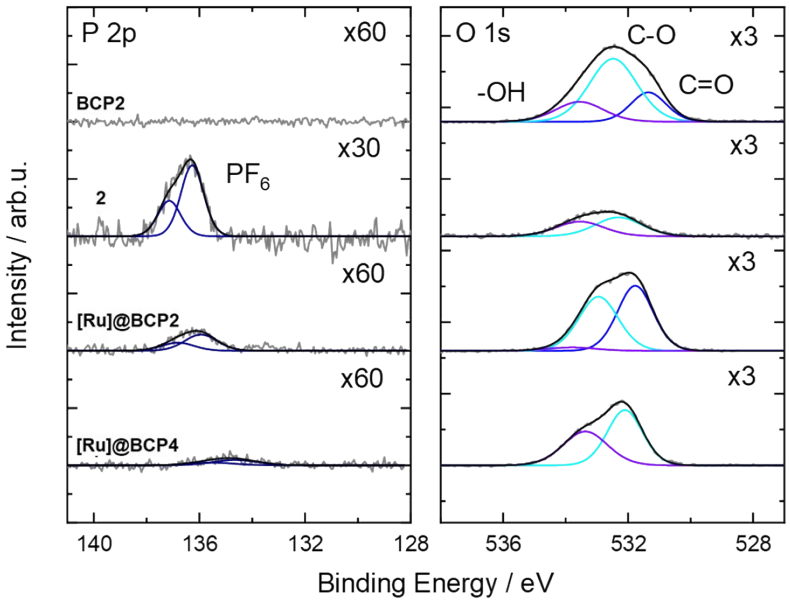

Figure S21: High resolution P 2p (left) and O 1s (right) XP spectra of PS_{277}-*b*-P(^{t}BuA_{262}-*co*-bpyEA_{28}) (**BCP2**), [Ru(bpy)$_2$(dmbpy)](PF_6)$_2$ (**2**), PS_{277}-*b*-P(^{t}BuA_{262}-*co*-bpyEA_{12}-*co*-([Ru(bpyEA)(bpy)$_2$](PF_6)$_2$)$_{16}$) (**[Ru]@BCP2**) and PS_{277}-*b*-P(AA_{262}-*co*-bpyEA_{12}-*co*-([Ru(bpyEA)(bpy)$_2$](CF_3CO_2)$_2$)$_{16}$) (**[Ru]@BCP4**). For better representation, intensities of the spectra are multiplied by a factor given in the figure with respect to the C 1s spectrum in Figure 4 of the main paper.

DLS data

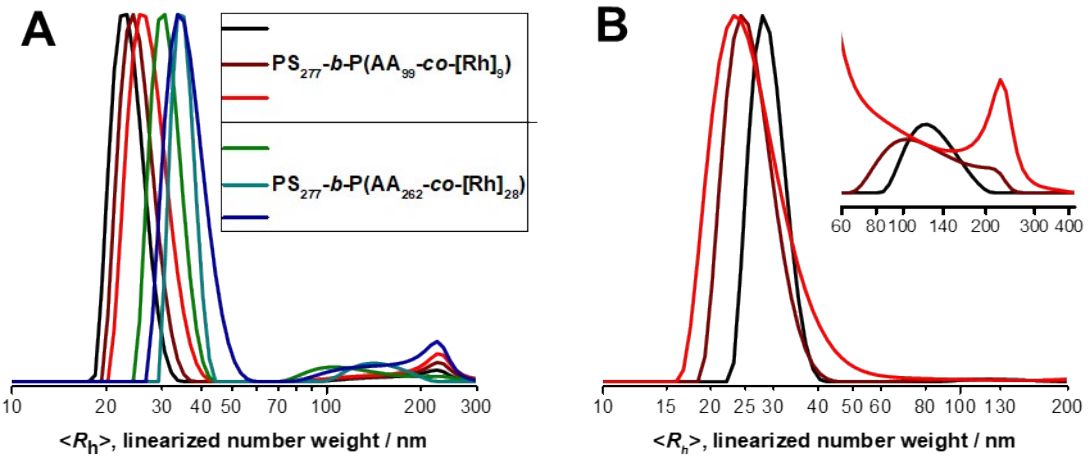

Figure S22: (**A**): DLS-CONTIN plots from three individual measurements for PS_{277}-*b*-P(AA_{99}-*co*-([Rh(bpyEA)(Cp*)Cl]CF_3CO_2)$_9$) (**[Rh]@BCP3**) (c = 0.3 g/L) and PS_{277}-*b*-P(AA_{262}-*co*-([Rh(bpyEA)(Cp*)Cl]CF_3CO_2)$_{28}$) (c = 0.4 g/L) (**[Rh]@BCP4**) based micelles in deionized water. Notably, second modes are observed between 70-200 nm with an additional artifact that is often seen for our setup around 226 nm. (**B**): DLS-CONTIN plots from three individual measurements for PS_{277}-*b*-P(AA_{262}-*co*-bpyEA_{12}-*co*-([Ru(bpyEA)(bpy)$_2$](CF_3CO_2)$_2$)$_{16}$) (**[Ru]@BCP4**) based micelles in deionized water, c = 0.5 g/L. Again, a second mode notable between 60-200 nm, accompanied again by an artifact around 226 nm can be observed.

TEM micrographs

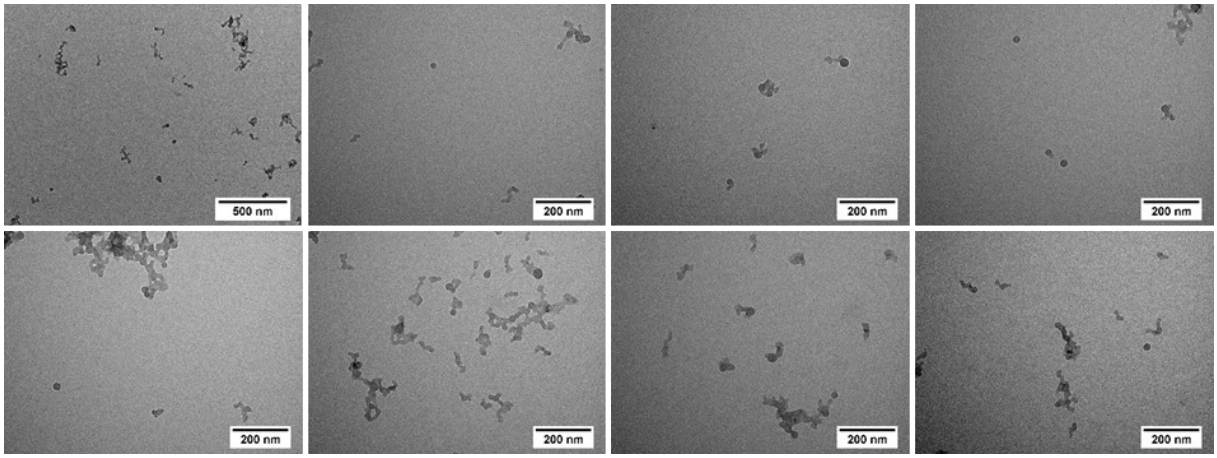

Figure S23: TEM images of PS_{277}-*b*-P(AA_{99}-*co*-([Rh(bpyEA)(Cp*)Cl]CF_3CO_2)$_9$) (**[Rh]@BCP3**) based micelles in deionized water, c = 0.3 g/L.

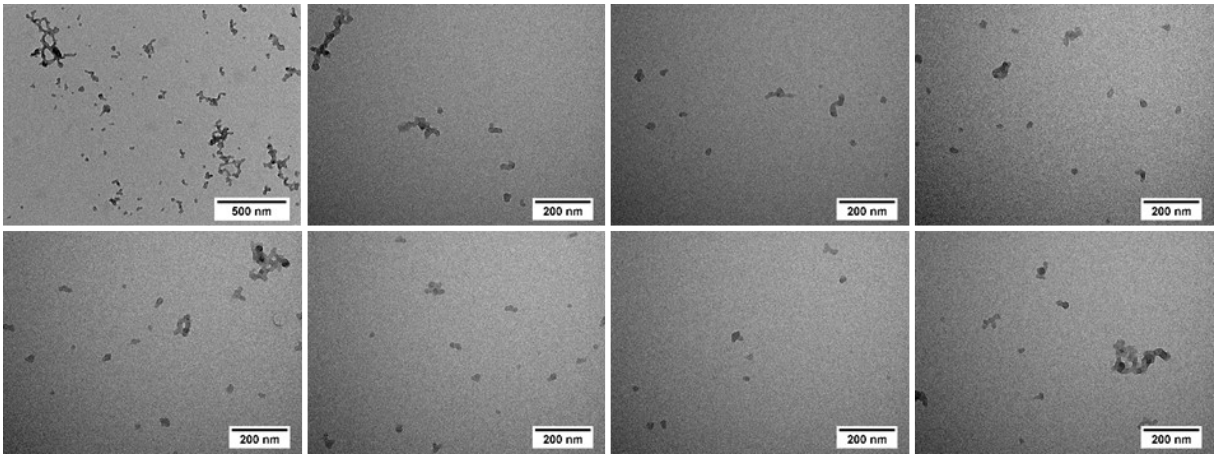

Figure S24: TEM images of PS_{277}-*b*-P(AA_{262}-*co*-([Rh(bpyEA)(Cp*)Cl]CF_3CO_2)$_{28}$) (**[Rh]@BCP4**) based micelles in deionized water, c = 0.4 g/L.

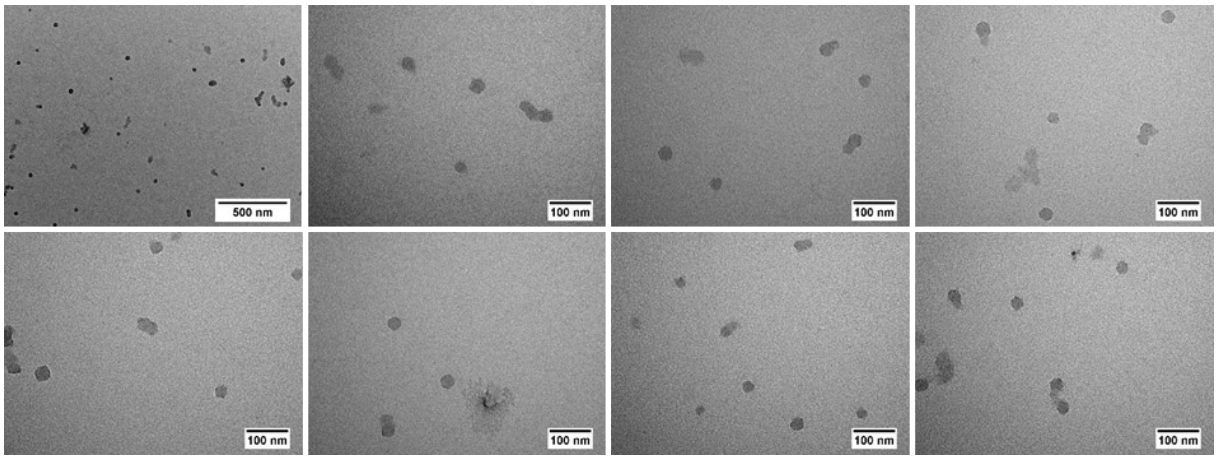

Figure S25: TEM images of of PS_{277}-*b*-P(AA_{262}-*co*-$bpyEA_{12}$-*co*-([Ru(bpyEA)$(bpy)_2$]$(CF_3CO_2)_2)_{16}$) (**[Ru]@BCP4**) based micelles in deionized water, c = 0.5 g/L.

STEM-EDX data

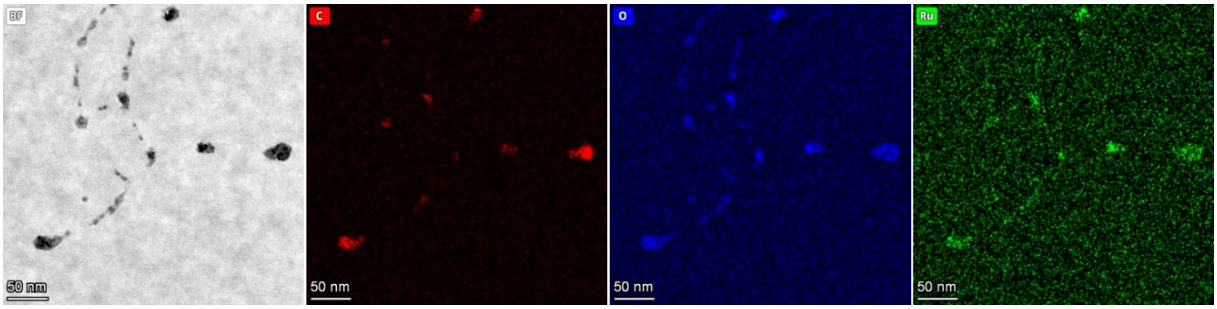

Figure S26: STEM-EDX analysis of [Ru]-micelles (**[Ru]@BCP4**) on SiN grids after O_2 plasma treatment, left to right: bright-field STEM image of deposited micellar residues; carbon mapping; oxygen mapping; ruthenium mapping.

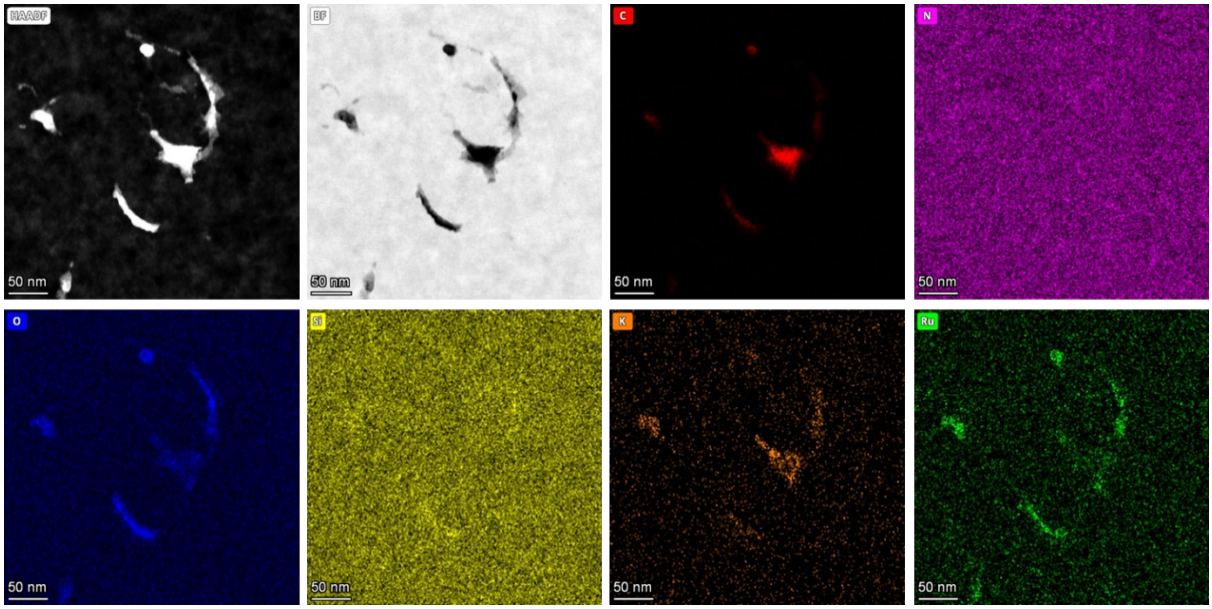

Figure S27: STEM-EDX analysis of [Ru]-micelles (**[Ru]@BCP4**) on SiN grids after O_2 plasma treatment. Top row, left to right: high-angle annular dark-field image, bright-field image, carbon mapping, nitrogen mapping; bottom row, left to right: oxygen mapping, silicon mapping, potassium mapping, ruthenium mapping.

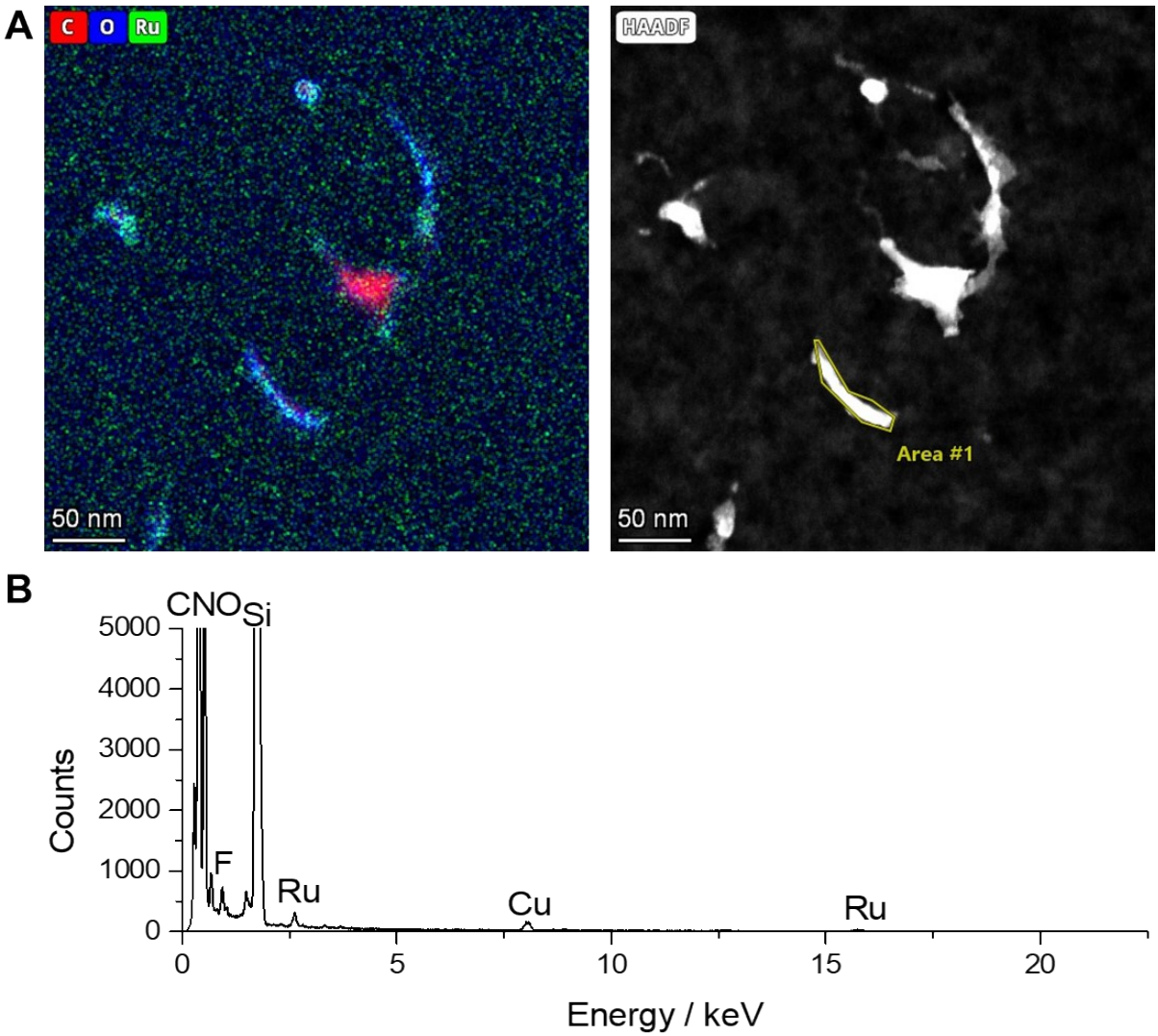

Figure S28: STEM-EDX analysis of [Ru]-micelles (**[Ru]@BCP4**) on SiN grids after O_2 plasma treatment. **A**: left: Color map superimposing the signals of carbon (red), oxygen (blue) and ruthenium (green) mappings, right: corresponding high-angle annular dark-field STEM image and highlighted area for spectral investigation. **B**: Extracted EDX spectrum of the area (marked in the A) showing the presence of Ru (L and K lines).

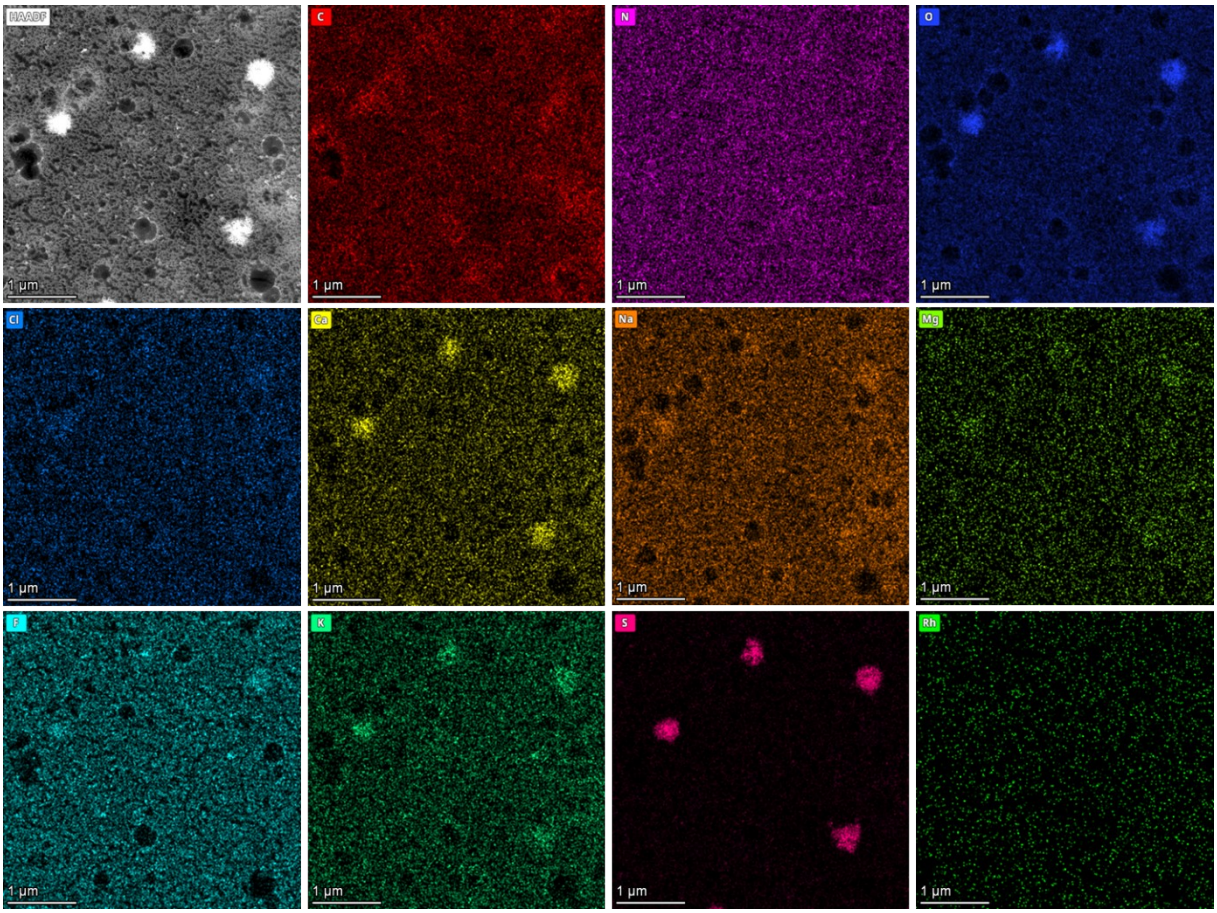

Figure S29: STEM-EDX analysis of [Rh]-micelles (**[Rh]@BCP4**) on SiN grids after O_2 plasma treatment. Top row, left to right: high-angle annular bright-field image, carbon mapping, nitrogen mapping, oxygen mapping; middle row, left to right: chlorine mapping, calcium mapping, sodium mapping, magnesium mapping; bottom row, left to right: fluorine mapping, potassium mapping, sulfur mapping, rhodium mapping.

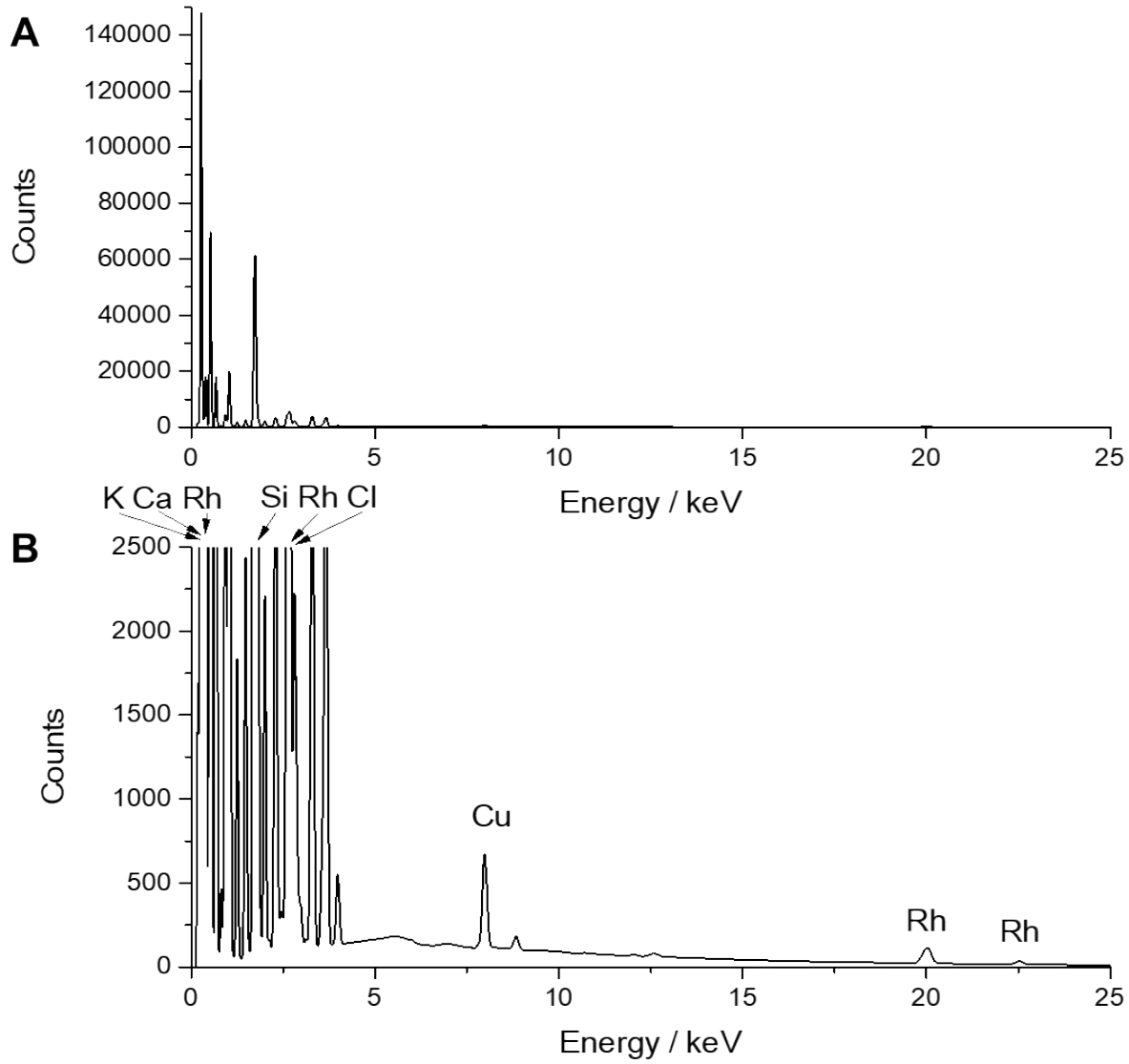

Figure S30: Extracted EDX spectra of an area from Figure S29 showing the presence of Rh, **A**: full range of intensity (counts), **B**: display of signals below 2500 counts and partial signal assignment.

Catalytic NAD^+ reduction studies

Table S3: (Photo)catalytic performance of [Rh] and [Ru] functionalized membranes as well as selected reference systems.

Entry	System	c ([Rh] or [Ru]) / µM	TON (after x min)	T / °C	reductant
1	**[Rh]@BCP3**	5 [Rh]	1.0 (90)	45	HCO_2^-
2	**[Rh]@BCP4**	5 [Rh]	1.0 (90)	45	HCO_2^-
3	**[Rh]@BCP3**	5 [Rh]	4.0 (90)	60	HCO_2^-
4	**[Rh]@BCP4**	5 [Rh]	4.0 (90)	60	HCO_2^-
5	**[Rh]@BCP3**	5 [Rh]	0.0 (90)	22	HCO_2^-
6	**[Rh]@BCP4**	5 [Rh]	0.0 (90)	22	HCO_2^-
7	**[Rh]+[Ru]@BCP5**	5 [Rh]	0.0 (30)	22	HCO_2^-
8	**[Rh]+[Ru]@BCP5**	5 [Rh], 5 [Ru]	1.8 (90)	45	HCO_2^-
9	[Rh(dmbpy)(Cp*)Cl]Cl (**1**)	5 [Rh]	15 (90)	22	HCO_2^-
10	[Rh(dmbpy)(Cp*)Cl]Cl (**1**)	5 [Rh]	40 (20)	45	HCO_2^-
11	**[Rh]@BCP3** and $[Ru(bpy)_3]Cl_2$	5 [Rh], 5 [Ru]	2.0 (90)	45	TEA
12	**[Rh]@BCP4** and $[Ru(bpy)_3]Cl_2$	5 [Rh], 5 [Ru]	2.0 (90)	45	TEA
13	**[Rh]@BCP4** and $[Ru(bpy)_3]Cl_2$	5 [Rh], 25 [Ru]	3.5 (120)	22	TEA
14	**[Rh]@BCP4** and $[Ru(bpy)_3]Cl_2$	5 [Rh], 25 [Ru]	4.5 (120)	45	TEA
15	**[Rh]@BCP4** and $[Ru(bpy)_3]Cl_2$	5 [Rh], 25 [Ru]	3.0 (120)	60	TEA
16	(**1**) and $[Ru(bpy)_3]Cl_2$	5 [Rh], 5 [Ru]	2.0 (90)	22	TEA
17	(**1**) and $[Ru(bpy)_3]Cl_2$	5 [Rh], 5 [Ru]	4.0 (90)	45	TEA
18	**[Rh]@BCP4** and $[Ru(bpy)_3]Cl_2$	5 [Rh], 5 [Ru]	1.7 (120)	22	TEA
19	**[Rh]@BCP3** and $[Ru(bpy)_3]Cl_2$	5 [Rh], 5 [Ru]	2.0 (120)	22	TEA
20	**[Rh]@BCP3** and $[Ru(bpy)_3]Cl_2$	5 [Rh], 5 [Ru]	2.0 (90)	45	TEA
21	**[Rh]@BCP4** and $[Ru(bpy)_3]Cl_2$	5 [Rh], 5 [Ru]	2.0 (90)	45	TEA
22	(**1**) and **[Ru]@BCP4**	5 [Rh], 5 [Ru]	0.8 (120)	22	TEA
23	**[Rh]@BCP4** and **[Ru]@BCP4**	5 [Rh], 5 [Ru]	0.4 (120)	22	TEA
24	**[Rh]+[Ru]@BCP5**	5 [Rh], 5 [Ru]	0.5 (120)	22	TEA

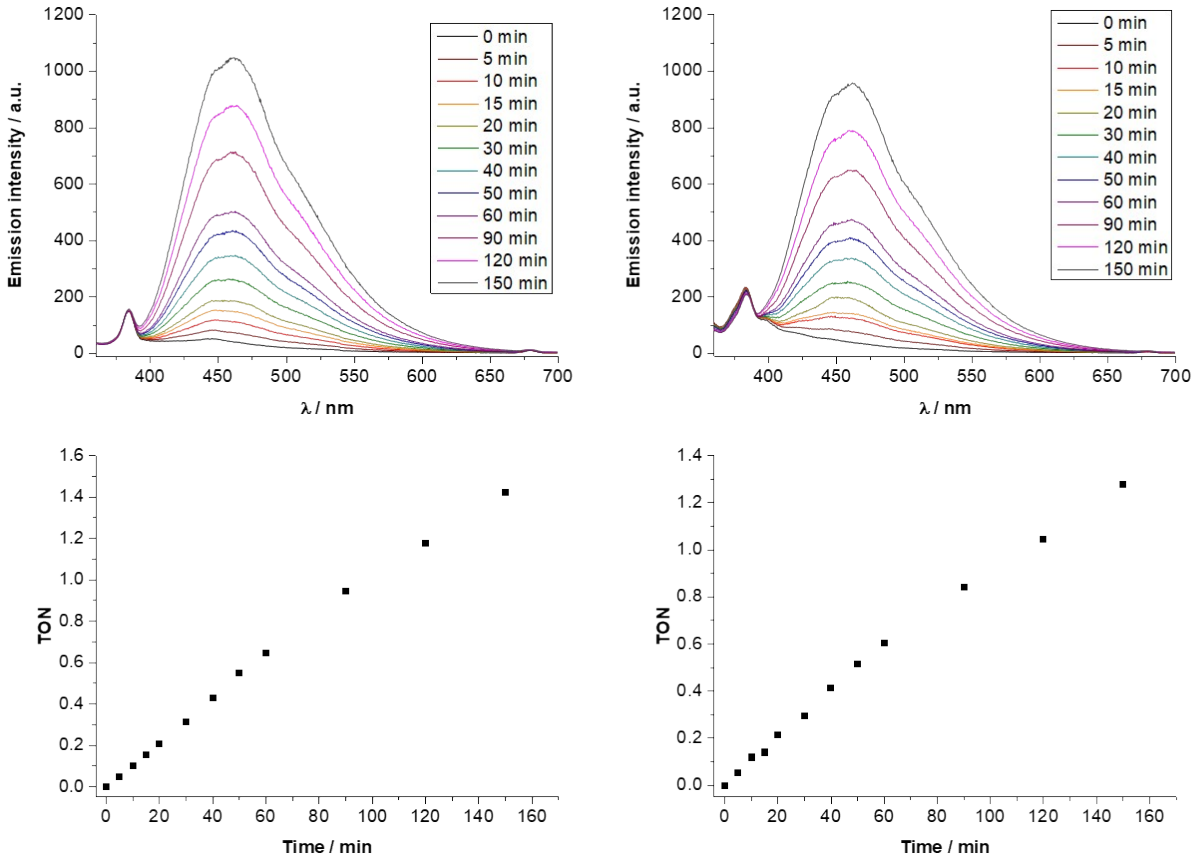

Figure S31: Emission spectroscopic changes (top row) and corresponding TON-plots (bottom row) during formate-driven NADH formation at 45°C using 5 µM [Rh] centers @ PS_{277}-*b*-P(AA_{99}-*co*-([Rh(bpyEA)(Cp*)Cl]CF_3CO_2)$_9$) (**[Rh]@BCP3**) (left column) and PS_{277}-*b*-P(AA_{262}-*co*-([Rh(bpyEA)(Cp*)Cl]CF_3CO_2)$_{28}$) (**[Rh]@BCP4**) (right column), respectively.

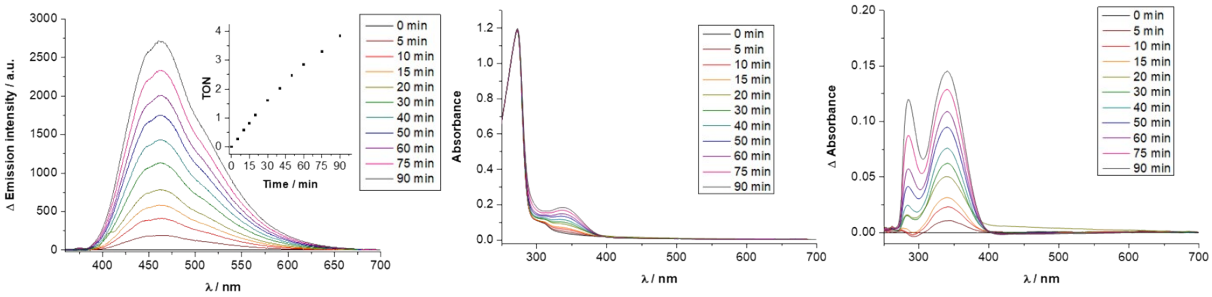

Figure S32: Emission (left) as well as UV/vis spectroscopic changes (center, right) during formate-driven NADH formation at 60°C using 5 µM [Rh] @ PS_{277}-*b*-P(AA_{99}-*co*-([Rh(bpyEA)(Cp*)Cl]CF_3CO_2)$_9$) (**[Rh]@BCP3**) (left) and 5 µM [Rh] @ PS_{277}-*b*-P(AA_{262}-*co*-([Rh(bpyEA)(Cp*)Cl]CF_3CO_2)$_{28}$) (**[Rh]@BCP4**) (center, right), respectively.

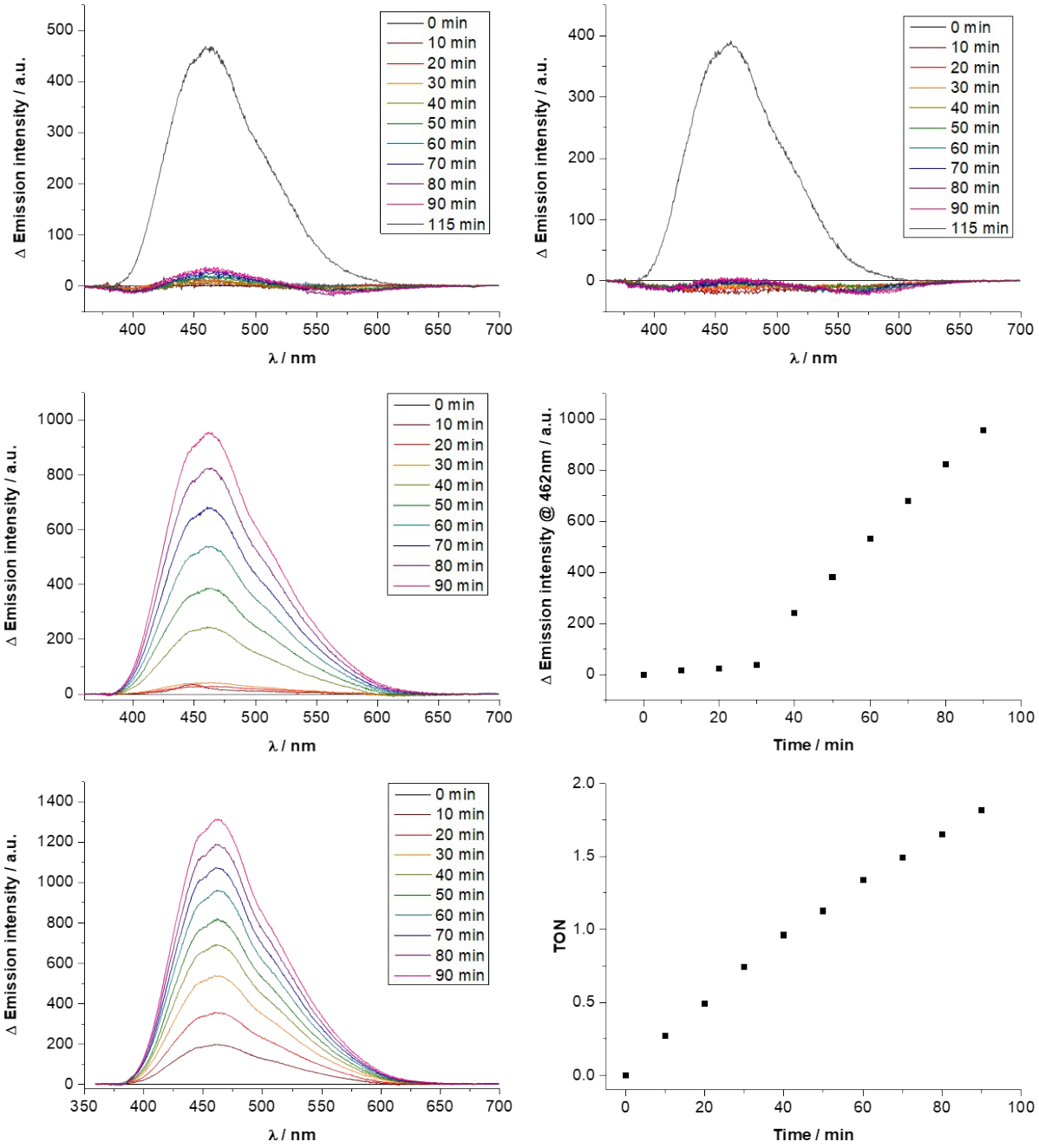

Figure S33: Emission spectroscopic changes during formate-driven NAD^+ reduction using either 5 µM [Rh] @ PS_{277}-*b*-$P(AA_{99}$-*co*-$([Rh(bpyEA)(Cp^*)Cl]CF_3CO_2)_9)$ (**[Rh]@BCP3**) (top left) or 5 µM [Rh] @ PS_{277}-*b*-$P(AA_{262}$-*co*-$([Rh(bpyEA)(Cp^*)Cl]CF_3CO_2)_{28})$ (**[Rh]@BCP4**) (top right) at r.t.. After 90 min each sample was placed for 25 min into a 45°C water bath. Middle row: Emission spectroscopic changes (left) and corresponding time *vs.* emission intensity plot (right) during the formate-driven NAD^+ reduction using 5 µM [Rh] @ PS_{277}-*b*-$P(AA_{262}$-*co*-$([Rh(bpyEA)(Cp^*)Cl]CF_3CO_2)_{12}$-*co*-$([Ru(bpyEA)(bpy)_2])$ $(CF_3CO_2)_2)_{16})$ (**[Rh]+[Ru]@BCP5**) (after 30 min the sample was placed into a 45°C water bath). Bottom row: Emission spectroscopic changes and corresponding TON-plot of the formate-driven NAD^+ reduction at 45°C using 5 µM [Rh] @ **[Rh]+[Ru]@BCP5**.

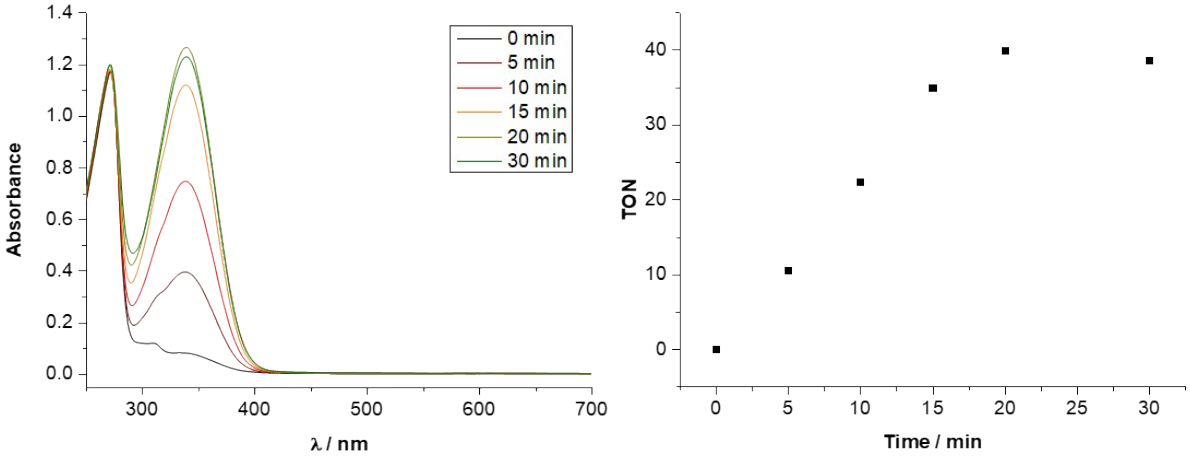

Figure S34: UV-vis spectroscopic changes during the formate-driven NAD^+ reduction using 5 µM [Rh(dmbpy)(Cp*)Cl]Cl at 45°C (left panel) and corresponding TON-plot (right panel).

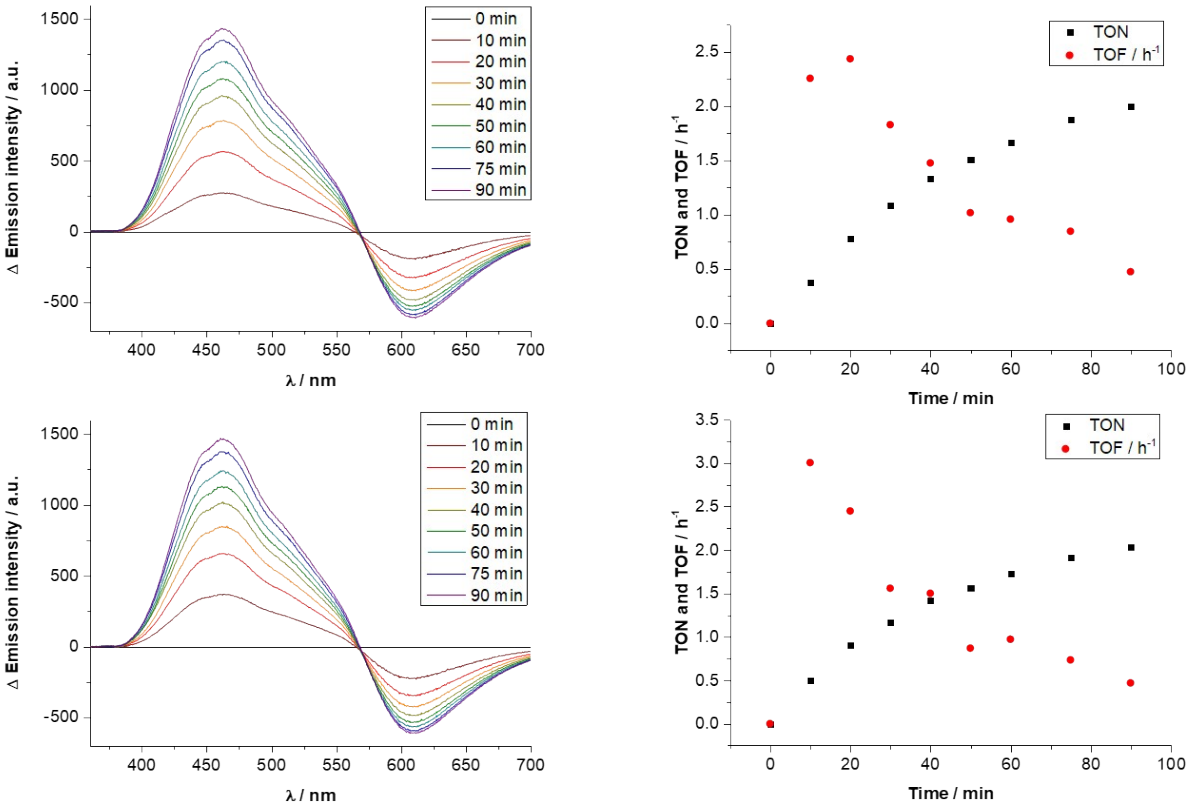

Figure S35: Emission spectroscopic changes (left) and corresponding TON- and TOF-plots (right) during photocatalytic NAD^+ reduction using 5 µM $[Ru(bpy)_3]Cl_2$ in combination with either 5 µM [Rh] @ PS_{277}-*b*-$P(AA_{99}$-*co*-$([Rh(bpyEA)(Cp^*)Cl]CF_3CO_2)_9)$ (**[Rh]@BCP3)** (top row) or 5 µM [Rh] @ PS_{277}-*b*-$P(AA_{262}$-*co*-$([Rh(bpyEA)(Cp^*)Cl]CF_3CO_2)_{28})$ (**[Rh]@BCP4)** (bottom row) at 45°C.

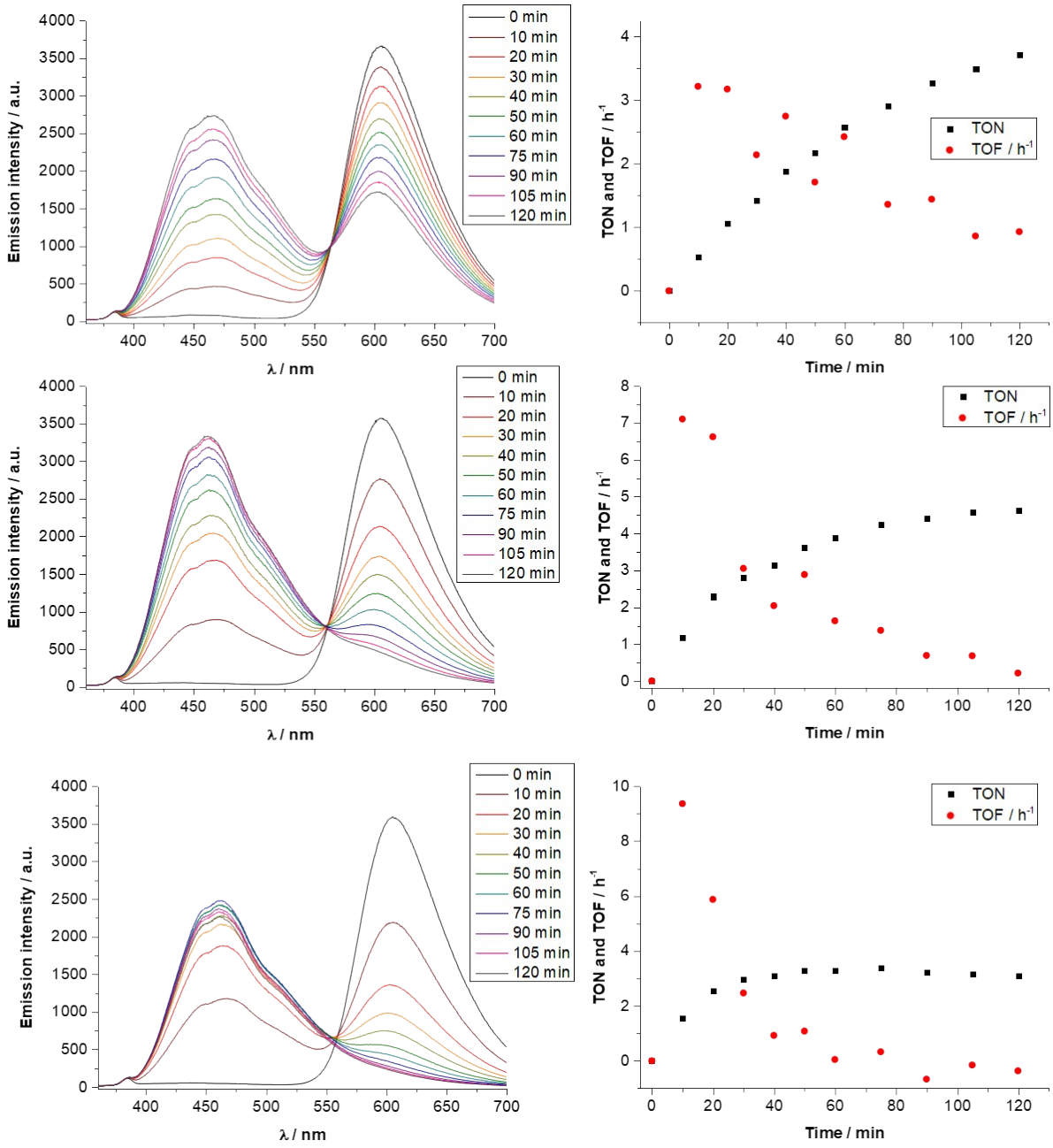

Figure S36: Emission spectroscopic changes (left column) and corresponding TON- and TOF-plots (right column) during photocatalytic NAD^+ reduction using 25 µM $[Ru(bpy)_3]Cl_2$ and 5 µM Rh @ PS_{277}-*b*-P(AA_{262}-*co*-([Rh(bpyEA)(Cp*)Cl]$CF_3CO_2)_{28}$) (**[Rh]@BCP4)** at r.t. (top row), 45°C (middle row) and 60°C (bottom row), respectively.

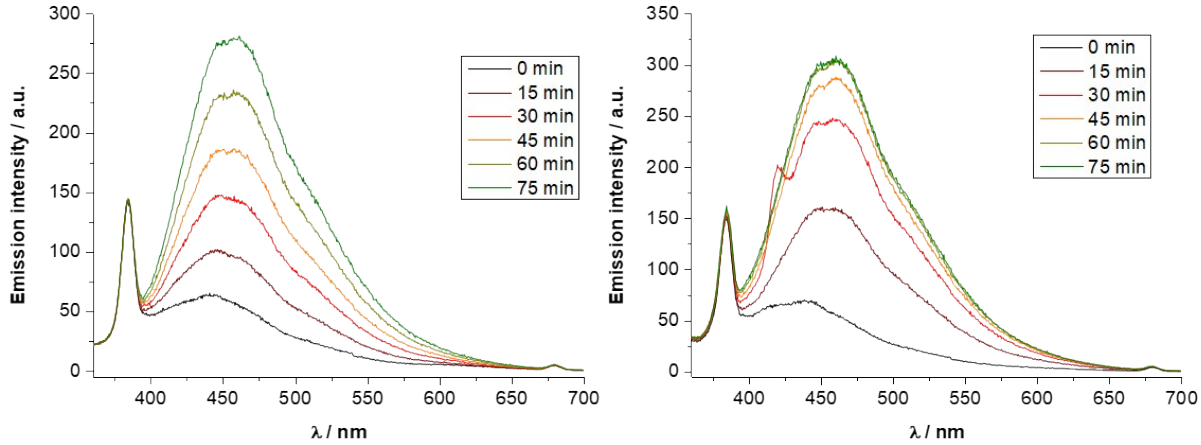

Figure S37: Emission spectroscopic changes during irradiation of 5 µM [Rh] @ PS_{277}-*b*-P(AA_{262}-*co*-([Rh(bpyEA)(Cp*)Cl]$CF_3CO_2)_{28}$) (**[Rh]@BCP4)** in presence of 250 µM NAD^+ in the typical buffer solution used for photocatalytic experiments at r.t. (left panel) and 60°C (right panel), respectively; no $[Ru(bpy)_3]Cl_2$ was added.

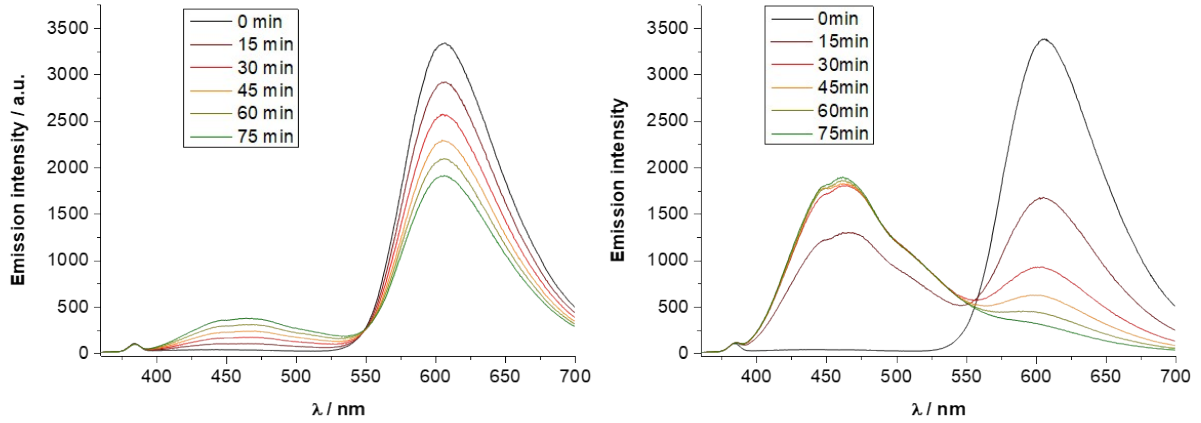

Figure S38: Emission spectroscopic changes during irradiation of 25 µM $[Ru(bpy)_3]Cl_2$ in presence of 250 µM NAD^+ in the typical buffer solution used for photocatalytic experiments at r.t. (left panel) and 60°C (right panel), respectively; no Rh catalyst was added.

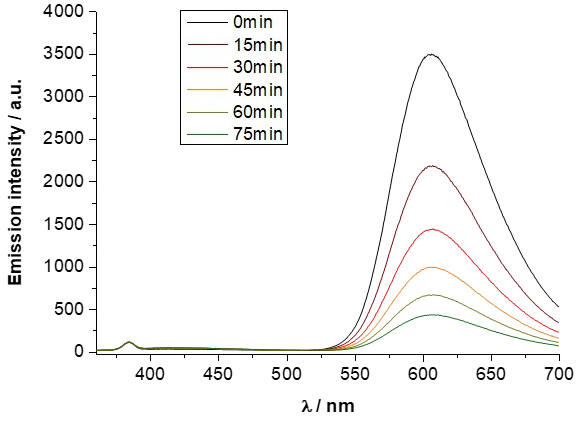

Figure S39: Emission spectroscopic changes during the irradiation of 25 µM $[Ru(bpy)_3]Cl_2$ in absence of any Rh catalyst as well as NAD^+. As solvent the typical buffer solution for photocatalytic experiments was utilized and the temperature was set to 60°C.

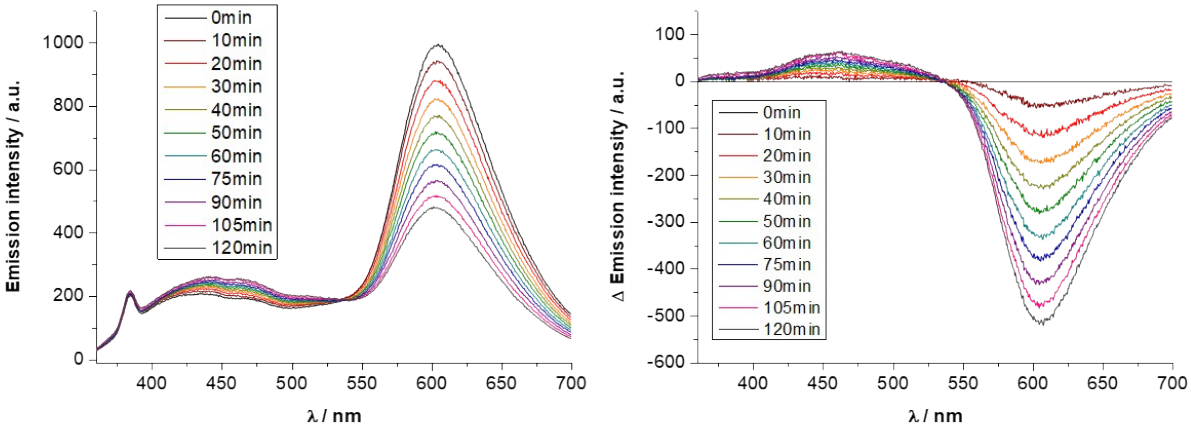

Figure S40. Emission spectroscopic changes during irradiation of 5 µM $[Ru(bpy)_3]Cl_2$ at r.t. in presence of 250 µM NAD^+ in the typical buffer solution used for photocatalytic experiments.

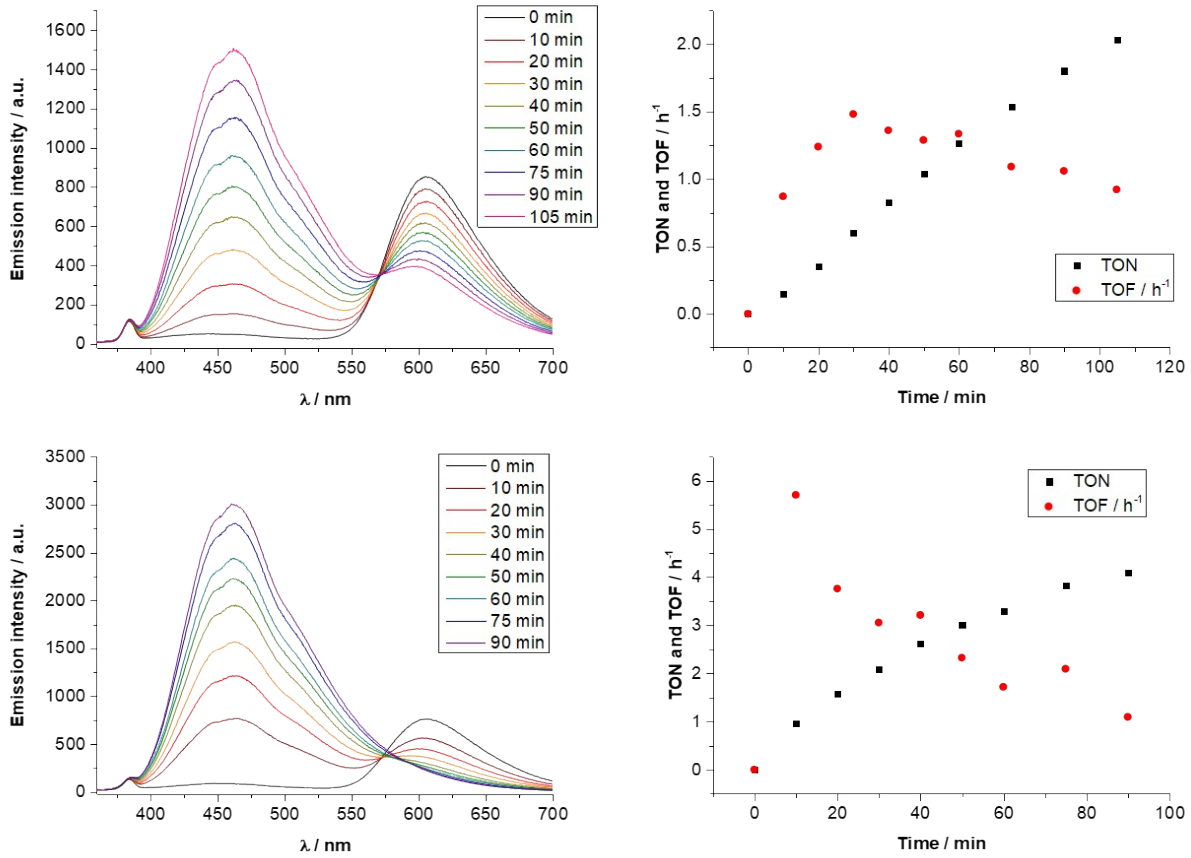

Figure S41: Emission spectroscopic changes (left column) and corresponding TON- and TOF-plots (right column) for the photocatalytic NAD^+ reduction using 5 µM $[Ru(bpy)_3]Cl_2$ and 5 µM [Rh(dmbpy)(Cp*)Cl]Cl at r.t. (top row) as well as at 45°C (bottom row), respectively.

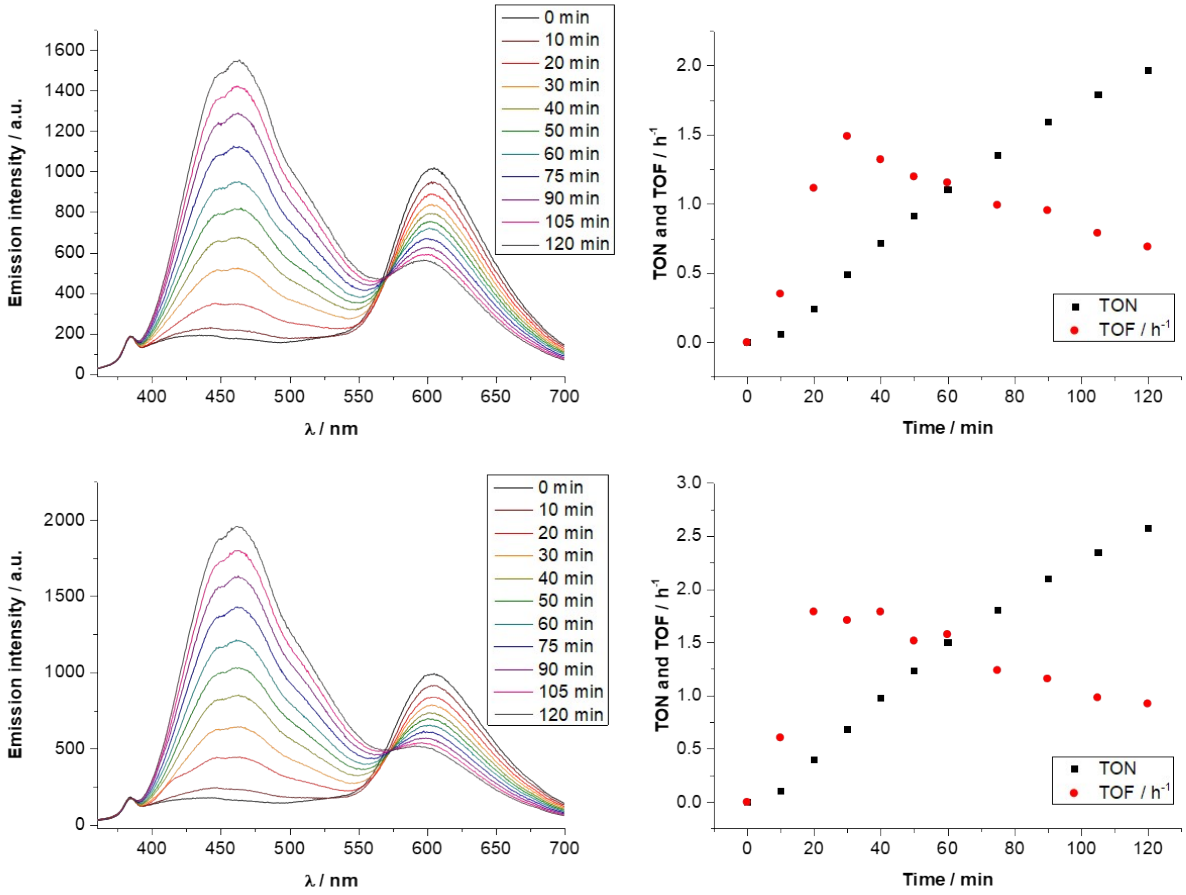

Figure S42: Emission spectroscopic changes (left column) and corresponding TON- and TOF-plots (right column) for the photocatalytic NAD^+ reduction at r.t. using 5 µM $[Ru(bpy)_3]Cl_2$ and 5 µM [Rh] @ PS_{277}-*b*-$P(AA_{262}$-*co*-$([Rh(bpyEA)(Cp^*)Cl]CF_3CO_2)_{28})$ (**[Rh]@BCP4)** (top row) or 5 µM [Rh] @ PS_{277}-*b*-$P(AA_{99}$-*co*-$([Rh(bpyEA)(Cp^*)Cl]CF_3CO_2)_9)$ (**[Rh]@BCP3)** (bottom row), respectively.

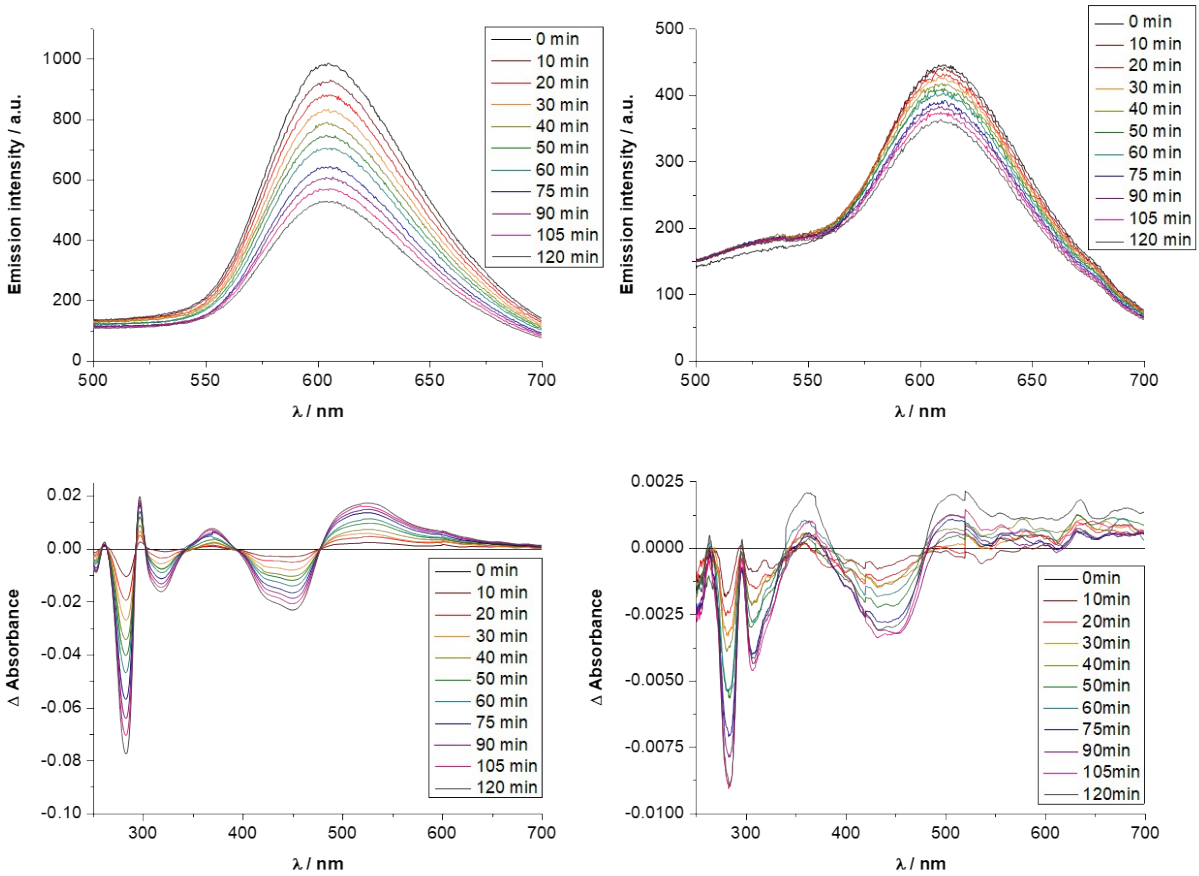

Figure S43: Emission spectroscopic (top row) as well as UV-vis absorption spectroscopic changes (bottom row) of 5 µM $[Ru(bpy)_3]Cl_2$ (left column) and 5 µM [Ru] @ PS_{277}-*b*-P(AA_{262}-*co*-$bpyEA_{12}$-*co*-([Ru(bpyEA)$(bpy)_2$]$(CF_3CO_2)_2)_{16}$) (**[Ru]@BCP4)** upon irradiation under typical photocatalysis conditions at r.t. (Ar-degassed water containing 0.12 M TEA and 0.1 M NaH_2PO_4).

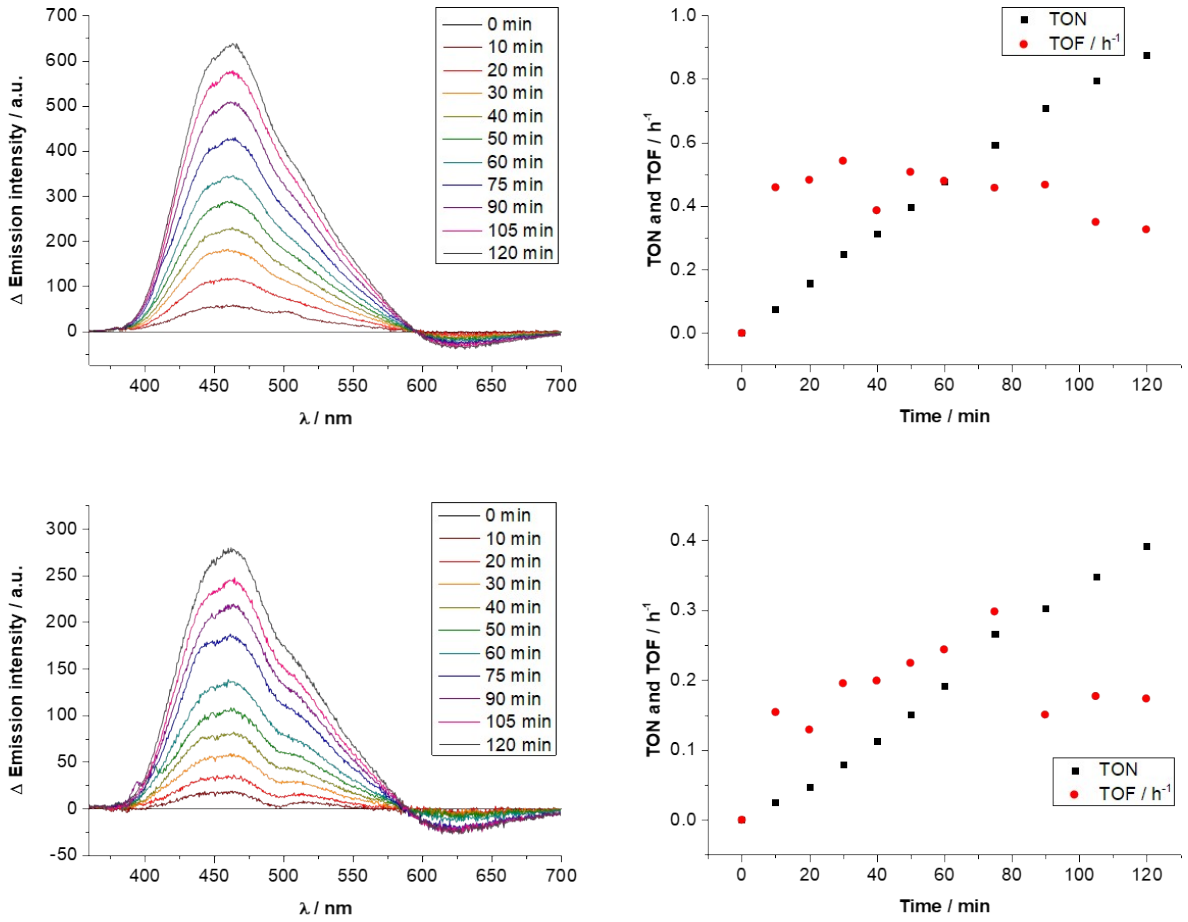

Figure S44: Emission spectroscopic changes (left column) as well as corresponding TON- and TOF-plots for the photocatalytic NAD^+ reduction at r.t. using 5 µM [Ru] @ PS_{277}-*b*-P(AA_{262}-*co*-bpyEA$_{12}$-*co*-([Ru(bpyEA)(bpy)$_2$](CF$_3$CO$_2$)$_2$)$_{16}$ (**[Ru]@BCP4)** together with either 5 µM [Rh(dmbpy)(Cp*)Cl]Cl (top row) or 5 µM [Rh] @ PS_{277}-*b*-P(AA_{262}-*co*-([Rh(bpyEA)(Cp*)Cl]CF$_3$CO$_2$)$_{28}$) (**[Rh]@BCP4)**, respectively.

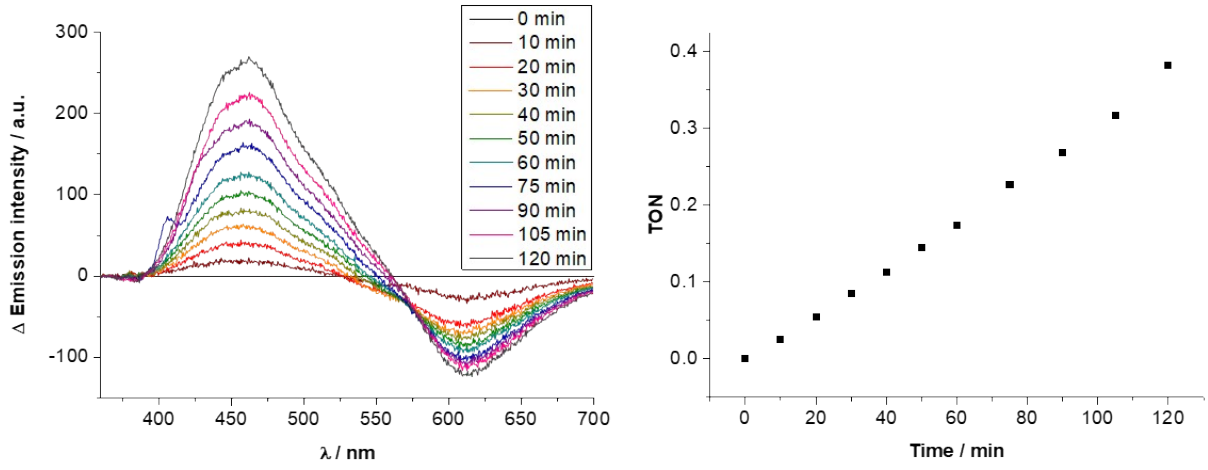

Figure S45: Emission spectroscopic changes (left) and corresponding TON-plot (right) upon irradiation of 5 µM [Ru] @ PS_{277}-*b*-P(AA_{262}-*co*-bpyEA$_{12}$-*co*-([Ru(bpyEA)(bpy)$_2$](CF$_3$CO$_2$)$_2$)$_{16}$ (**[Ru]@BCP4)** within the typical buffer solution containing 250 µM NAD^+.

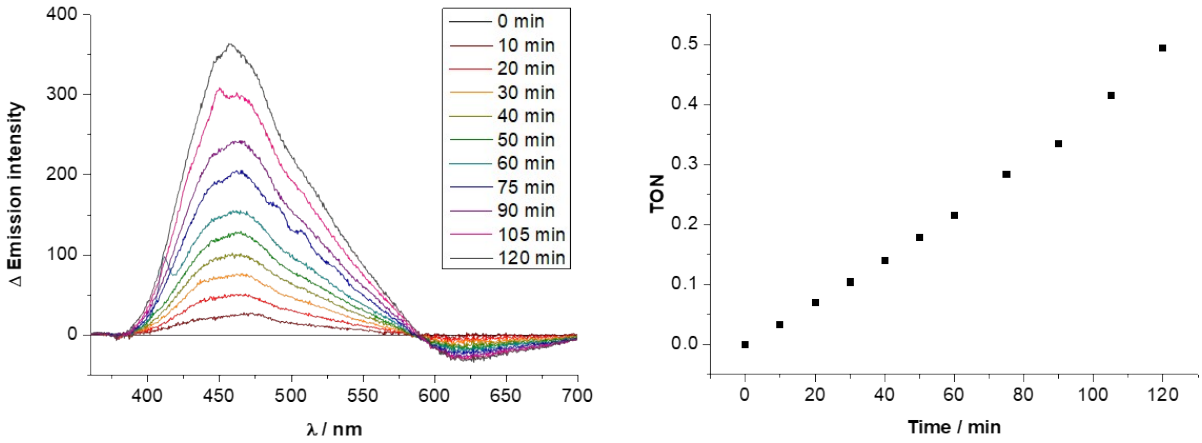

Figure S46: Emission spectroscopic changes (left) and corresponding TON-plot (right) upon irradiation of 5 µM [Ru] and 5 µM [Rh] @ PS_{277}-*b*-P(AA_{262}-*co*-([Rh(bpyEA)(Cp*)Cl]$CF_3CO_2)_{12}$-*co*-([Ru(bpyEA)(bpy)$_2$]) $(CF_3CO_2)_2)_{16}$) (**[Rh]+[Ru]@BCP5)** within the typical buffer solution containing 250 µM NAD^+.

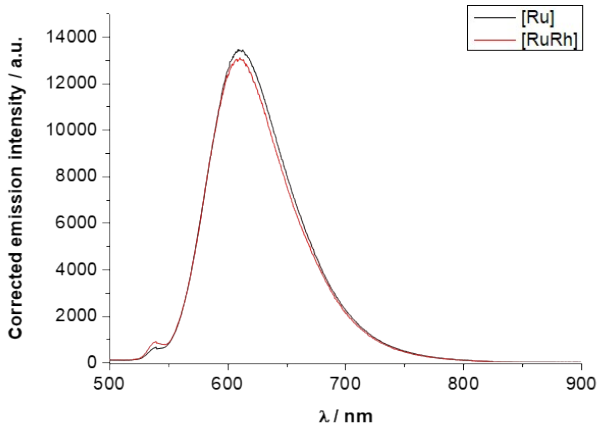

Figure S47: Emission spectra of 5 µM [Ru] @ PS_{277}-*b*-P(AA_{262}-*co*-bpyEA$_{12}$-*co*-([Ru(bpyEA)(bpy)$_2$]$(CF_3CO_2)_2)_{16}$ (**[Ru]@BCP4**), black curve) and 5 µM [Ru] and [Rh] ([RuRh]) @ PS_{277}-*b*-P(AA_{262}-*co*-([Rh(bpyEA)(Cp*)Cl]$CF_3CO_2)_{12}$-*co*-([Ru(bpyEA)(bpy)$_2$]) $(CF_3CO_2)_2)_{16}$) (**[Rh]+[Ru]@BCP5**), red curve) in degassed H_2O under Ar atmosphere (the emission intensities were corrected for the absorbance of the individual samples at the chosen excitation wavelength (450 nm)).

S6 Supplementary references

[1] L. Zhang, R. J. Barlow, A. Eisenberg, *Macromolecules* **1995**, *28*, 6055.

[2] J. Eichhorn, Y. D. Gordievskaya, E. Y. Kramarenko, A. R. Khokhlov, F. H. Schacher, *Macromolecules* **2021**, *54*, 1976.

[3] A. Ito, N. Kobayashi, Y. Teki, *Inorg. Chem.* **2017**, *56*, 3794.

[4] M. G. Pfeffer, B. Schäfer, G. Smolentsev, J. Uhlig, E. Nazarenko, J. Guthmuller, C. Kuhnt, M. Wächtler, B. Dietzek, V. Sundström, S. Rau, *Angewandte Chemie (International ed. in English)* **2015**, *54*, 5044.